Cytological and genetic consequences for the progeny of a mitotic catastrophe provoked by Topoisomerase II deficiency.

Cristina Ramos-Pérez[1,2,†], Margaret Dominska[3], Laura Anaissi-Afonso[1,2], Sara Cazorla-Rivero[1,2], Oliver Quevedo[1,‡], Isabel Lorenzo-Castrillejo[1], Thomas D Petes[3,*] and Félix Machín[1,4,*]

[1] Unidad de Investigación, Hospital Universitario Nuestra Señora de Candelaria, Santa Cruz de Tenerife, Spain.

[2] Universidad de La Laguna, Tenerife, Spain.

[3] Department of Molecular Genetics and Microbiology, Duke University Medical Center, Durham, NC, USA.

[4] Instituto de Tecnologías Biomédicas, Universidad de La Laguna, Tenerife, Spain.

[†] Present address: BenchSci Analytics Inc., Toronto, Canada.

[‡] Present address: Nucleolar Stress and Disease Group. Genomic integrity unit. Danish Cancer Society Research Center, Copenhagen, Denmark.

* Corresponding authors:

Félix Machín. Unidad de Investigación, Hospital Universitario Nuestra Señora de la Candelaria, Ctra del Rosario 145, 38010 Santa Cruz de Tenerife, Spain. Tfno: +34 922 602 951. E-mail: fmachin@funcanis.es

Thomas D Petes. Department of Molecular Genetics and Microbiology, Duke University Medical Center, 213 Research Dr., Durham, NC 27710. E-mail: tom.petes@duke.edu

ABSTRACT

The interplay between regulated cell death (RCD) and mitotic catastrophe (MC) determines much of the success of many anticancer treatments. Down-regulation of Topoisomerase II (Top2) is the more direct and devastating form of MC since it happens concomitantly with the formation of anaphase bridges in cells proficient for G_2/M checkpoints. Herein, we have characterized in budding yeast the consequences for the cell progeny of a *top2* MC. Clonogenic and microcolony experiments, in combination with vital stains, showed that 75% of daughter cells become senescent immediately after the *top2* MC; they are unable to divide but remain alive. Decline in cell vitality occurred slowly, not even reaching 50% of cells 24 h after the MC, and uncoordinatedly when comparing pairs of daughters. Genetic experiments showed that the RCD mediator Mca1/Yca1 does not modify the senescence/death outcome. We thus conclude that MC mediated by Top2 deficiency leads to short-term senescence that eventually ends up in non-regulated cell death. Furthermore, we showed that the ability to divide in the short term can be modulated by the chromosome ploidy, suggesting that gross chromosome imbalances during segregation may account for senescence in the *top2* progeny. Indeed, we found that diploid long-term survivors of the *top2* MC are prone to genomic imbalances such as trisomies, uniparental disomies and terminal loss of heterozygosity (LOH), the latter affecting the longest chromosome arms.

Keywords: Mitotic catastrophe, Top2, anaphase bridges, cell death, cell vitality, senescence, genomic instability, uniparental disomy, loss of heterozygosity.

INTRODUCTION

Mitotic catastrophe (MC) is a class of cell death still poorly understood, and with a conflictive definition among the scientific community [1–4]. In its most general acceptation, we can consider MC as the cell-death-triggering event that follows an aberrant mitosis. This aberrant mitosis requires that cells are committed to segregate the duplicated genome to the daughter cells under conditions that preclude the success of such attempt. MC is presumed to be of the outmost importance in cancer biology, both as an oncosuppressive barrier in carcinogenesis and a mechanism of cell death after anti-cancer treatments. Many antitumor drugs that damage the DNA or the microtubules lead to chromosome segregation failures provided that cells do not stop their division cycle in a timely fashion [5–7]. Human cells make use of p53, ATM, ATR, p38/MK2 and Mps1, among other proteins, to arrest the cell cycle in G_1/S or G_2/M following DNA damage and other genome-altering events, and tumour cells frequently lack one or several of these checkpoint proteins [8–11]. When checkpoints are functional, cancer cells treated with DNA- or microtubule-damaging agents often die after a transient cell cycle arrest through a regulated cell death (RCD) known as intrinsic apoptosis [12,13]. Cancer cells are more prone to die than healthy cells because they grow more rapidly and are often deficient in repair systems that could eventually overcome the inflicted damage. Apoptosis causes the permeabilization of the mitochondrial outer membrane, and the subsequent leakage of pro-apoptotic factors into the cytosol [3]. Execution of the intrinsic apoptosis is significatively accelerated by the activation of the so-called caspase-mediated transduction cascade. When checkpoints or apoptosis are non-functional, MC is expected to take over. Therefore, understanding MC is becoming increasingly important in cancer biology.

MC is expected to kill most of the progeny due to major genomic imbalances and massive irreparable DNA damage. However, whether MC might also trigger a form of RCD or, rather, it simply leads to an accidental cell death (ACD) is still unclear. In addition, MC is reported to lead to senescence in certain backgrounds [1,14]. Senescence refers to the irreversible cell cycle arrest of otherwise live cells. Significant differences in the outcome are expected for MCs that result from different sources. Thus, MC occurring upon microtubule damage likely leads to missegregation of whole chromosomes prior to cell death, whereas DNA damage can give rise to more complex outcomes. For instance, DNA damage may result in either breakage of the DNA molecule (i.e, double strand breaks, DSBs) or replication stress (i.e., stalled replication forks). Attempts to segregate broken chromosomes would yield daughter cells with irreparable damage. Attempts to segregate underreplicated chromosomes would cause the formation of anaphase bridges (ABs), which may end up in DSBs upon cytokinesis with the same deleterious consequences [15–18]. Another condition that leads to MC concomitant with the appearance of ABs occurs when catenations between sister chromatids persist until anaphase. This happens when the catalytic action of topoisomerase II (Top2) is downregulated [19–22]. Top2 downregulation seems to pass undetected by cell cycle checkpoints in many cancer cell lines but not in normal differentiated cells [22–29]. Consequently, catalytic inhibition of Top2 offers a promising target to promote MC in cancer cells irrespective of the status of DNA damage G_1/S and G_2/M checkpoints [30]. Of note, Top2 is often downregulated during acquisition of secondary resistance to chemotherapeutical regimes that comprise Top2 poisons, a major class of antitumor drugs that generate Top2-mediated DSBs [31,32]. This observation implies that these resistant cancer cells should become even more hypersensitive to inhibition of Top2.

Top2 is essential in all organisms. In *Saccharomyces cerevisiae*, inactivation of Top2 by means of thermosensitive (ts) alleles leads to MC in anaphase without previous checkpoint activation [20,33–36]. In recent years, *S. cerevisiae* has also been a model to study both cell death pathways and genomic instability footprints after environmental or genetic insults [37,38]. Here, we have characterized the consequences for the offspring of inactivating Top2 through the *top2-5* ts allele (hereafter refer to as *top2* MC). We show that most of the *top2* MC progeny lose their ability to divide. Interestingly, these daughter cells do not die abruptly but, rather, there is a slow decline in cell vitality over several hours. The patterns of cell death point towards an ACD, which was genetically corroborated with mutants for the main apoptotic pathway. We have also used heterozygous diploids to diagnose chromosome rearrangements in the surviving progeny, and we found genomic footprints that include uniparental disomy and terminal loss of heterozygosity in the longest chromosome arms. We conclude that (i) most *top2* daughter cells become senescent in the short-term while eventually dying by ACD; and (ii) the surviving offspring frequently carry genomic rearrangements expected from transiting through anaphase with unresolved sister chromatids.

RESULTS.

Most of the immediate progeny of a *top2-5* mitotic catastrophe irreversibly stops cell division.

We have recently reported that the *top2-5* thermosensitive mutant undergoes timely progression through the cell cycle until a MC occurs in late anaphase [36]. Importantly, *top2-5* gives a clear point-of-no-return in the MC phenotype because cytokinesis makes the *top2-5* anaphase bridges collapse irreversibly. In many ways, this MC is similar to other previously studied *top2* conditional alleles [20,35], although *top2-5* provides a better synchrony through the MC since a larger percentage of cells quickly sever the anaphase bridge [36]. This particularity might be connected to a better inactivation of Top2-5 at 37 ºC, as predicted from the number and classes of mutations in the *top2-5* allele (Fig. S1). Single-cell videomicroscopy showed that mother and daughter cells struggled to rebud (the most obvious yeast signal for a new cell cycle) after the MC, at least during the first six hours. Indeed, rebudding only happened in 20% of the mothers, leading to a microcolony of just three cell bodies [36]. We hereafter refer to cell bodies rather than cells or buds since it is difficult to conclude whether they are part of a single multi-budded cell, a budded mother with a daughter or a mother with two daughters.

In our previous work [36], we filmed cells on agarose patches by fluorescence microscopy using GFP-labeled histones to follow nuclear segregation. Concerned that the outcome of the experiment might be affected by the modest doses of UV irradiation and/or the hypoxic conditions in the patch, we repeated the experiment with cells grown on the surface of agar within a Petri dish and photographed through long-range objectives. We found the same outcome (Fig. 1A) as in our previous study. Whereas *TOP2* G_1/G_0 cells were

able to form microcolonies of around 10 cell bodies after 6 h at 37 ºC, *top2-5* cells stopped dividing at either 2 (~65%) or 3 (~20%) cell bodies. This 2-3 cell-body pattern was an end-point phenotype upon continuous Top2 inactivation, since we observed the same proportions after 24 h at 37 ºC (Fig. 1B). Next, we investigated whether reactivation of Top2 by shifting the temperature down to 25 ºC would allow any of these bodies to divide (re-bud) again. In order to have an overall picture of cell viability, we first determined clonogenic survival after different incubation periods at 37 ºC. Because of the complexity of the budding patterns after the MC, we chose a clonogenic assay that allows to determine if at least one of the cell bodies was still viable by the time of the temperature shift, no matter how many cells are present in the progeny (Fig. 1C). We found that *top2-5* had a gradual loss of viability (50% survival after ~ 4 h), and less than 5% clonogenic survival was obtained after 24 h at 37 ºC; the *TOP2* isogenic strain retained the expected 100% clonogenic survival in this assay (data not shown).

Because in these clonogenic assays there is a mixture of budded and unbudded cells at the time of plate seeding, we repeated the clonogenic survival after 6 h at 37º C, but photomicrographing the plate surface at different time points. Through this analysis, we determined that at time 0 h the unbudded:budded ratio was 2:1; however, only half of the surviving macrocolonies came from unbudded cells (Fig. 1D). This result implies that the chance to become a macrocolony is doubled if the original cell was budded at the time of the temperature upshift. The most likely explanation for this bias resides in the fact that the *top2* MC is expected to be milder if cells are closer to anaphase onset when Top2 is inactivated. Indeed, budded cells appeared to better complete the first two cell cycles at the restrictive conditions (Fig. S2). Therefore, we hereafter mostly focused on those cells which were in G_1/G_0 at the time of the temperature upshift. A calculation based on the cell proportions at 0h (66% G_1/G_0), overall macrocolony formation from the 37 ºC for 6h regime (~25%), and the

155 origin of those macrocolonies (50% from G_1/G_0) led us to conclude that around ~20% of the
156 original G_1/G_0 cells gave rise to survivors after 6 h at 37 ºC [0.25 × 0.5 / 0.66 = 0.2].

157 Next, we tried to correlate the long-term clonogenic survival of the G_1/G_0 cells with
158 their ability to form microcolonies. We reasoned that it is possible that many MCs could
159 render viable progeny in the short-term (microcolony) but could not raise a visible colony
160 later (macrocolony). This difference could reflect a gradual loss of viability in the progeny as
161 a consequence of genomic imbalances acquired after the MC. To get further insights into this
162 possibility, we took pictures of the cells on the surface of Petri dishes at the time of seeding
163 (0h), right after the 37 ºC incubations (6h or 24h), and 16 h or 24 h after the plates were
164 shifted back to 25 ºC (Fig. 2A). As expected from above, most of the original G_1/G_0
165 (unbudded) cells did not go beyond the 2-3 bodies stage during the 37 ºC incubations (Fig.
166 2A, B; inner circles in the sunburst plots). Restoring permissive conditions for Top2 activity
167 allowed very few of the cell progeny to divide again (Fig. 2A, B; outer circles in the sunburst
168 plots). This finding was true not only during the long (24 h) incubation at 37 ºC, but also for
169 the 6 h incubation. Thus, only ~15% of the 2-3 cell bodies observed after 6 h at 37 ºC were
170 able to re-bud again once or more after incubating them back at 25 ºC. Incidentally, a low but
171 significant proportion of G_1/G_0 cells did not bud during the 37 ºC regimes. However, even in
172 these non-MC cases, cells did not divide after the Top2 reactivation, suggesting that this
173 G_1/G_0 subpopulation was already incapable of cell division following growth at 25 ºC.

174 Longer incubations at 25 ºC after the MC resulted in microcolonies of >50 cells that
175 eventually developed into macrocolonies. With our cell density settings, microcolonies of
176 more than 20-30 cells hindered us from raising conclusions about the fate of adjacent cells.
177 However, the position of the center in these microcolonies suggests that most, if not all, of

178 the G_1/G_0 cells that ended up as macrocolonies had re-budded again within the first 24 h that
179 followed the temperature downshift.

180 From previous analysis by videomicroscopy, we know that most *top2-5* doublets (2
181 bodies) and all triplets (3 bodies) have passed anaphase and thus completed a MC after 6 h at
182 37 ºC [36]. Nevertheless, we decided to complete the analysis of the immediate progeny by
183 testing whether the observed cell bodies have accomplished cell separation. Our reasoning
184 was that separation by micromanipulation would demonstrate that cell bodies have become
185 individual daughter cells. Indeed, we could separate with the needle more than half of the
186 doublets and triplets (Fig. 2C, middle concentric circle in the sunburst chart). We next tried to
187 correlate the ability of all these cells to form macrocolonies but found that they were largely
188 unviable. The percentage of macrocolonies was much lower than expected, indicating that
189 that micromanipulation likely kills cells that otherwise would have retained viability.

190 We conclude from this set of experiments that yeast *top2* MC irreversibly
191 compromises the short- and long-term ability to divide for more than 75% of the cell
192 progeny.

193

194 **Cell death after prolonged absence of Top2 activity occurs slowly, asynchronously,**
195 **asymmetrically and is independent of the Yca1 metacaspase.**

196 We noticed from the microcolony experiments performed above that cells swelled
197 after prolonged incubations at 37 ºC (Fig. 2A). After 24 h at 37 ºC, the volume occupied by
198 the original mother cell doubled (Fig. 3A). Downshift of the temperature to 25 ºC only
199 modestly deflated these cells. In addition, a low proportion of cell bodies underwent lysis

("0"; 2 → 1 and 3 → 2 categories in previous sunburst charts). These findings led us to consider osmotic stress due to the continuous growth in size of the mother cell as a possible cause underlying the long-term inviability and/or short-term inability to divide of the *top2* progeny. However, addition of 1.2 M sorbitol, an osmotic stabilizer, neither prevented cells from swelling (Fig. 3A) nor improved long-term viability (Fig. 3B) or short-term division capability (Fig. 3C).

Next, we analysed cell bodies in these microcolonies more closely, seeking other morphological patterns of cell disease aside from swelling; for example, lysis, darkening and loss of the rounded shape (Fig. 4A). Most of these morphological features have been previously related to different forms of cell death. Because the *top2-5* strain also carries a GFP-labeled H2A histone, we also monitored nuclear morphology and chromatin integrity (i.e., GFP intensity). Cells still looked fully healthy after 6 h at 37 ºC (no difference with 0 h), despite the great loss in the ability of the progeny to divide. Only after prolonged 37 ºC incubations did the cells start to look clearly sick. Still, more than 50% of cell bodies harboured a nuclear GFP signal even 24 h following the 37 ºC upshift. This GFP signal co-existed in cell progenies that showed unhealthy patterns in the bright field such as swelled, darkened, or non-rounded cell bodies.

In order to better study cell death after *top2* MC, we employed other means that required experiments to be performed in liquid media instead of Petri dishes. We first quantified the rate of cell death and metabolic decline by staining with the vital dye methylene blue (MB) (Fig. 4B). This dye stains dead cells blue; and it can also stain cells that are alive but metabolically attenuated [39]. A time course after the 37 ºC upshift showed that there was not a major increase in MB positive cell bodies in the first 4 h (the equivalent in

liquid cultures to 6 h on solid medium; [36]). In general, the increase in MB+ bodies was linear, but even 24 h after the 37 ºC upshift ~40% of cell bodies were not stained by MB. These staining experiments uncovered two other properties of the *top2* MC: i) it was common that only one cell body was MB+ in doublets and triplets (Fig. S3A); and ii) both unbudded and budded cells were stained (Fig. S3B). Regarding the former, the result suggest that loss of vitality is not coordinated between mother and daughter(s) cells. This asymmetry also confirms that many doublets must have completed cytokinesis despite remaining together. As for the latter, the staining pattern suggests that loss of vitality occurs in an asynchronous fashion in terms of any preference for a cell cycle stage.

Because MB does not distinguish whether cell bodies are dead or simply metabolically stressed, we next sought other more informative vital stains. Firstly, we employed the fluorescent vitality probe FUN1©. This probe stains metabolically active live cells with red vacuolar aggregates [40]. FUN1© is considered more informative and reliable than MB. With this probe we confirmed that only ~10% of cell bodies have lost vitality after just 4 h at 37 ºC (left chart of Fig. 4C; Fig. S4). It was also surprising that vitality decline still affected no more than 40% of all cell bodies after 24 h at 37 ºC.

We also used Propidium Iodide (PI) to monitor cell viability. Loss of plasma membrane impermeability is considered a *bona fide* marker of cell death [37]. PI is only able to fluorescently stain cells that have lost such impermeability. Anticipating some sort of RCD after the *top2* MC, we decided to accompany PI staining in red with a reporter for reactive oxygen species (ROS) in green. Intrinsic ROS production has been observed during RCD in all eukaryotes, including yeast, and is considered one of most reliable RCD markers [41]. After overnight growth at 25 ºC (0h), the *top2-5* strain had neither dead cells nor cells with

246 ROS (right part of Fig. 4C, Fig. S5). Four hours after the 37 ºC temperature shift, there was
247 only a slight increase in dead cell bodies (~6%) and almost no signs of ROS in the rest
248 (~3%). Only after 24 h of incubating the cells at 37 ºC, we found a significant proportion of
249 both ROS (~20%) and dead cells (~20%). It is noteworthy that the percentage of PI+ cells
250 was still relatively low after this 24 h incubation, and 60% of all cell bodies were still
251 resistant to PI and free of ROS.

252 We next examined if the observed dead cells after the *top2* MC were the result of a
253 regulated suicidal (apoptotic) process or the result of accidental (non-regulated) death. In
254 order to address these possibilities, we deleted the only caspase-like gene in yeast,
255 *YCA1/MCA1*. Yca1 is required for apoptosis in yeast in response to several environmental
256 stresses [42–44]. In addition to cell death, we checked whether Yca1 modulated the other
257 behaviours seen in the *top2* MC progeny (for example, the inability to divide and the slow
258 decline in cell vitality). The conclusions raised from comparing *top2-5 YCA1* and *top2-5*
259 *yca1*Δ were that Yca1/Mca1: (i) had no influence in the percentage or rate of cells that end up
260 dying (Fig. 4B, C); (ii) neither accelerated nor slowed down the vitality decline (Fig. 4B, C);
261 (iii) did not modify the profile of clonogenic survival after the *top2* MC (Fig. 4D); and (iv) its
262 absence did not improve the ability of the immediate cell progeny to divide (Fig. 4E).

263 The overall conclusion from these experiments is that the immediate progeny of the
264 *top2* MC enter a senescent-like state as they retain vitality but loses their ability to re-bud.
265 Senescence is only a transient state that last several hours or days, until cells eventually die.
266 The pattern of cell death (morphologically diverse, slow, asynchronous and asymmetrical)
267 together with the lack of effect of Yca1 suggest that loss of Top2 leads to ACD.

268

Chromosome ploidy modulates the ability of the progeny to divide.

All the experiments described above were carried out in haploid yeast cells. In haploids, MC associated with the presence of partly unresolved sister chromatids, as in the *top2-5* mutant, is expected to be highly deleterious. Severing of these anaphase bridges result in daughter cells that may lack several chromosome arms [18]. Based on this consideration, one might expect that diploid cells would be more resistant to the consequences of *top2* MC than haploid cells. Thus, we studied the *top2* MC in an isogenic homozygous *top2-5/top2-5* diploid (2N) strain. Unlike its haploid counterparts, diploid cells were more often able to re-bud at least once. In fact, ~50% of all 2-3 cell bodies originated from just after 6h at 37 ºC were able to do so after the 25 ºC downshift (Fig. 5A). This percentage dropped considerably if the progeny was incubated 24 h at 37 ºC. Strikingly, however, the increase in the ability to divide again after the MC did not yield better clonogenic survival (Fig. 5B), indicating that most of this viable progeny was competent to re-bud only in the first generations. We also performed a microdissection analysis of the diploid *top2* progeny. Unlike haploid *top2-5* cells, which was rather sensitive to micromanipulation, 13% of the diploid progeny raised a macrocolony after the separation attempt (Fig. 5C). Altogether, we conclude that a *top2* MC in diploids results in better short-term ability to divide.

Genome instability footprints in the surviving progeny from the *top2*-mediated mitotic catastrophe.

Above, we have just shown that ~25% of the *top2-5* diploid cells still gave rise a macrocolony after the 6h at 37ºC regime. We next examined the genomes of these survivors

in search for specific genomic footprints of the *top2* MC. To accomplish this goal, instead of using the homozygous isogenic diploid employed in the previous chapter, we generated a highly heterozygous hybrid *top2-5* diploid. The hybrid diploid was generated by crosses of two sequence-diverged *top2-5* haploids, derivatives of W303-1A and YJM789, which are heterozygous for more than 55,000 single-nucleotide polymorphisms (SNPs) distributed throughout the yeast genome (the yeast genome is 15 Mb). These heterozygous SNPs allow the analysis of various types of genomic alterations by using SNP-specific microarrays [45,46]. Each SNP array contains 25-base oligonucleotides that matched either the W303-1A-associated allele or the YJM789-associated allele for about 13,000 different SNPs. By measuring the relative amounts of hybridization to each oligonucleotide, we could detect loss of heterozygosity (LOH) (an event expected from mitotic recombination), as well as analyse deletions, duplications, and changes in chromosome number. Examples of this type of analysis will be described further below.

The hybrid diploid was also engineered to select various types of chromosome alterations on chromosome V (Fig. 6A). The, diploids were homozygous for the *ade2-1* mutation on chromosome XV (an ochre-suppressible allele) and heterozygous for the *SUP4-o* suppressor gene in chromosome V [47]. Strains with the *ade2-1* mutation form red colonies in YPD in the absence of the *SUP4-o* suppressor. Diploid strains with one or two copies of *SUP4-o* form pink and white colonies, respectively [48]. Thus, loss of the *SUP4-o* gene by mitotic recombination (to be discussed later) or chromosome loss results in a red colony instead of the pink colonies characteristic of the original strain. Colony colour changes are also expected if the copy number of the *ade2-1* allele varies by loss or duplication of chromosome XV. In addition, aneuploidy for other chromosomes sometimes alters the color of the colony. As will be described further below, we analysed genomic alterations under two

315 types of conditions: (i) in colonies that were derived from cells incubated at 37 ºC for 6 h,
316 plated at the permissive temperature without regard to colony color and (ii) in red/white
317 sectored colonies derived from cells incubated under the same conditions as the unsectored
318 colonies.

319 The hybrid *top2-5* strain FM1873 is homozygous for the *top2-5* mutation.
320 Microcolony and clonogenic experiments showed that this strain lost viability quicker than
321 the isogenic homozygous diploid in the S288C background (Fig. 6B, C). There was a steady
322 rise in red and/or red/white sectored colonies among the survivors during the 37 ºC
323 incubation, as expected if the *top2* MC increases genome instability (Fig. 6D). We used
324 microarrays to examine genomic alterations in the control FM1873 isolate (no exposure to 37
325 ºC) and in isolates exposed to 37 ºC for 6 h, and then allowed to form colonies at 25 ºC. It is
326 important to stress that the SNP microarrays allow analysis of genomic alterations throughout
327 the genome in addition to those changes that occur on chromosome V [45,46]. Examples of
328 microarrays for some types of genomic changes are shown in Fig. 7. In the left side of the
329 figure, the Y-axis shows the normalized hybridization ratio to probes specific to the W303-
330 1A form of the SNP (red) or the YJM789 form of the SNP. Heterozygous SNPs have ratios of
331 about 1 (details in Materials and Methods); in LOH events, SNPs derived from one homolog
332 have a ratio of near 2 and those derived from the other have a ratio near 0. One common
333 pattern is a terminal LOH (T-LOH) event (Fig. 7A). As shown on the right side of the figure,
334 this pattern can reflect a reciprocal crossover. Alternatively, T-LOH events can occur by a
335 non-reciprocal type of recombination termed “break-induced replication” (BIR, not shown)
336 [49]. A second type of LOH is an interstitial LOH event (I-LOH; Fig. 7B) in which a region
337 of LOH is flanked by heterozygous. I-LOH events (gene conversions) result from the non-
338 reciprocal transfer of DNA sequences between homologs. Two other classes of genomic

339 rearrangements are a consequence of chromosome non-disjunction. Such non-disjunction
340 events can result in trisomy (Fig. 7C) or monosomy. An event in which one homolog is
341 duplicated and another deleted is called "uniparental disomy" (UPD) and can reflect a non-
342 disjunction event in which the two homologs segregate into different daughter cells (Fig. 7D).

343 When the control FM1873 strain was examined before exposure to the restrictive
344 temperature, surprisingly, we found that it was altered relative to an isogenic *TOP2*/*TOP2*
345 hybrid [49]. More specifically, we realized that FM1873 carried a terminal LOH (t-LOH) on
346 the right arm of chromosome XII (the longest chromosome arm in yeast). In addition, all
347 isolates had three to four copies of chromosome XIV. We tried several times to recreate the
348 hybrid *top2-5* diploid but were unable to isolate a derivative that had only two copies of XIV.
349 Since this chromosome is the location of *top2-5*, it is likely that chromosome XIV trisomes
350 and tetrasomes have a selective growth advantage over the diploids that have only two *top2-5*
351 copies even at the permissive temperature. We generated an isogenic derivative of FM1873
352 (MD684) that lacked the T-LOH event on XII, although it still had extra copies of XIV. For
353 our subsequent genomic analyses, we studied both FM1873 and MD684.

354 The experimental strains were exposed to the restrictive temperature of 37 ºC by
355 incubating the cells for six hours either on plates or in liquid (details in Materials and
356 Methods); these two protocols resulted in similar levels of instability. A total of 27 isolates
357 were examined for FM1873 (13 experimental, 14 control), and 19 isolates of MD684 (10
358 experimental, 9 control). Somewhat surprisingly, the control single-colony isolates (cells not
359 exposed to 37 ºC) also had high rates of instability (Table 1; "C" samples), indicating that the
360 Top2p encoded by *top2-5* does not have wild-type activity even at the permissive
361 temperature. Indeed, a previous biochemical study reported that the Top2-5 activity at 25 ºC

362 is 33% of that of wild type Top2 [50]. Among all isolates examined, we found 76 T-LOH
363 events, 3 I-LOH events, 31 trisomies, 2 monosomies, and 6 UPDs.

364 The average number of genetic changes per strain (including all the data of Table 1) was
365 3.3 alterations/isolate. Since the strains were grown approximately 40 generations before
366 microarray analysis, the rate of alterations/cell division/isolate is about 8.3×10^{-2}. In a
367 previous microarray analysis of a wild-type diploid isogenic with FM1873 and MD684, we
368 found a rate of alterations of about 2×10^{-3}/division, a rate about 40-fold less than for the
369 *top2* strains. The most common alteration in the *top2* strains was a terminal LOH event (64%
370 of the total events). These events likely reflect the repair of a DSB by either a crossover or a
371 BIR event (Fig. 7). The chromosomal distribution of the events is striking. The right arms of
372 chromosome IV and XII (the two longest arms in the yeast genome) had over 80% of the
373 terminal LOH events (60/76), although these arms represent less than 30% of the yeast
374 genome. Other chromosomes with terminal LOH events (the number of events shown in
375 parentheses) are: XIII (5), XV (4), VII (3), XIV (2), VII (1), XI (1), and V (1). Chromosomes
376 XIII, XV and XIV have the third, fourth, and fifth longest chromosome arms in the genome,
377 respectively; all of the mapped events in these chromosomes are on the longest arms.
378 Strikingly, the very large (about 1.2 Mb) ribosomal RNA gene cluster (rDNA) on the right
379 arm of chromosome XII was not a preferred site for terminal LOH events. Although the
380 rRNA gene cluster is about 60% of the right arm of XII, only 30% (3 of 11) of the LOH
381 events had a breakpoint in or near the rRNA genes. We should point out that terminal LOH
382 events on XII could only be followed in the MD684 strains (FM1873 already had a cXIIr T-
383 LOH); hence, our estimate of the frequency of terminal LOH events on the right arm of XII is
384 a minimal estimate.

In addition to LOH events, we observed 33 changes in chromosome number (31 trisomies and 2 monosomies) (Table 1). The frequencies of trisomies are not simply related to the size of the chromosomes. Chromosomes V, VIII, and XV were the most frequently-observed trisomes; chromosomes V and VIII are medium-sized chromosomes (both about 550 kb), whereas chromosome XV is large (1092 kb). Only one trisomy was observed involving one of the three smallest chromosomes (I, VI, and III). Only three of the trisomies involved the two largest chromosomes IV and XII. A straightforward explanation of the large number of trisomic chromosomes is that the intertwining of sister chromatids in the *top2* strains often results in their co-segregation into one of the daughter cells.

We also observed six UPD events (Fig. 7D). In strains with these events, the homolog is present in two copies, but both copies are derived from one of the original parental homologs. There are two plausible pathways to generate UPD (Fig. S6): two non-disjunction events in different cell cycles or reciprocal UPD (RUPD) in which one pair of homologs segregates into one cell and the other pair segregates into the other cell. Although both pathways probably contribute to UPD in yeast, at least some of the events in wild-type strains are RUPD [51]. To determine whether RUPD events occurred frequently in the *top2* cells, we used a protocol in which both daughter cells produced as a result of RUPD or a reciprocal crossover (RCO) in chromosome V could be recovered in different sectors of a sectored colony (Fig. S7). The sectored colonies were derived from the same strains (FM1873 and MD684) used for our single-colony analysis. As discussed previously, a crossover or RUPD can produce a red/white sectored colony. However, to select for such events, both FM1873 and MD684 contained a heterozygous *can1-100* marker located allelically to the *SUP4-o* insertion and a gene encoding hygromycin resistance (*hph*) located distal to the *can1-100* insertion. The *can1-100* mutation is a nonsense mutation, and is suppressed by *SUP4-o*.

Strains that lack the suppressor are resistant to the drug canavanine and those with the suppressor are sensitive. A crossover between *can1-100* and the centromere results in formation of a canavanine-resistant red/white sectored colony (Fig. S7A); a sectored colony with the same phenotype can also result from RUPD (Fig. S7B). RCO and RUPD events can be distinguished by microarray analysis (bottom panels of Fig. S7).

Following exposure of FM1873 and MD684 to 37 ºC, we found 242 red/white Can^R sector colonies, 43 of which had the sectoring pattern for the *hph* marker suggestive of RCO or RUPD events. We found both RCO and RUPD events in two-thirds of these colonies (Table S1). The rate of RUPDs in cells of FM1873 and MD684 treated for six hours at 37 ºC was the same, 1.1 x 10^{-5}/division; the rate of RUPD in cells of FM1873 that were not exposed to 37 ºC was 1 x 10^{-6}. The rate of RCO in FM1873 cells treated at 37 ºC was 2.7 x 10^{-6}; no RCO events were observed in MD684. In an isogenic wild-type strain, the rates of RUPD and RCO for chromosome V were 10^{-7} and 1.6 x 10^{-6}, respectively [51]. These results support the conclusion that the *top2* mutation results in a substantially elevated rate of RUPD (about 100-fold) and has little effect on the rate of RCO.

DISCUSSION

The formation of anaphase chromosome bridges during the cell division is one of the most dramatic sources of genetic instability. Too many bridges are expected to cause a kind of mitotic catastrophe (MC) which will kill the progeny. Downregulation of topoisomerase II (Top2) is likely the most common way of generating large numbers of anaphase bridges. In addition, downregulation of Top2 has important implications during acquisition of resistance

against cancer therapy that comprises Top2 poisons (for example, etoposide and anthracyclines). In the present work, we have studied the consequences of downregulating Top2 in yeast. We show that the expected MC often leads to progeny unable to divide; however, cell death is not immediate but the result of a decline in cell vitality that takes hours to complete. We further propose that the irreversible genomic imbalances that occur during chromosome segregation in the absence of Top2 explain the short-term senescence observed in the immediate progeny. This hypothesis is strengthened by the observation that diploid survivors of a *top2* MC often carry genomic footprints expected from anaphase bridges such as uniparental disomies and terminal loss of heterozygosity. A step-by-step summary of the events ensuing the *top2* MC is shown in Fig. 8.

On the short-term cytological consequences of the *top2* mitotic catastrophe.

In this study we have adopted the term mitotic catastrophe (MC) in its broadest cytological sense, referring to aberrant mitoses that are expected be deleterious for the progeny based on the degree of observed abnormalities. It is worth mentioning that other authors, especially those working with metazoans, restrict the MC term to death occurring in mitosis after a mitotic insult, while using terms such as mitotic slippage to refer to an aberrant chromosome segregation following a mitotic insult [3,52]. With this restriction in mind, MC in metazoans is a sort of RCD, whereas mitotic slippage could result in cell death, either RCD or ACD, or lead to survivors. In our yeast experimental model with the *top2-5* allele, death before anaphase is insignificant since cells go through G_2/M and anaphase as quickly as their *TOP2* counterparts [36]. Nevertheless, other *top2* alleles appear to block cells in G_2/M either by activating the spindle assembly checkpoint (SAC) or the DNA damage/replication checkpoint [35,53]; it would be interesting to closely follow the fate of these blocked cells,

454 although cell death was not reported in the short-term. In nocodazole-treated cells, which also
455 arrest cells in G_2/M by activation of SAC, 40% cell death has been reported after 10 h in
456 clonogenic assays [54]. This cell death was described to occur through an RCD apoptosis-like
457 mechanism.

458 Our clonogenic assays showed that a sudden drop in viability occurs between 3-6 h
459 after Top2 inactivation (Fig 1C), about the time needed for cells to complete telophase and
460 cytokinesis on solid medium [36]. From the microcolony experiments, we concluded that the
461 ensuing *top2-5* progeny are largely impaired in entering a second cell cycle (Fig 1A, B and
462 2). This impairment can be partly alleviated in diploids, yet only in the short-term (Fig 5).
463 This observation leads us to propose that gross genomic imbalances prevent the immediate
464 progeny from cell cycle progression. Taking into account previous reports on the formation
465 of anaphase bridges in *top2-ts* mutants [20,36] and high levels of chromosome
466 missegregation [34], it appears logical that many of the haploid progeny lose entire
467 chromosomes containing essential genes. In addition, loss of essential genes may reflect
468 breakage of chromosomes at the bridge followed by loss of the distal chromosome regions
469 [18,55].

470 An interesting third scenario is that daughter cells immediately die upon the *top2* MC
471 through an RCD program. This would imply that either mitotic cells or their immediate
472 progeny sense the MC and execute an RCD, as in metazoans and in nocodazole-blocked
473 yeast cells [14,54]. Our results, however, argue against this possibility. Firstly, many cells
474 stained negative for death markers (PI) and positive for metabolic activity (FUN1©) even
475 after 24 h at 37 ºC. Secondly, the decline in cell vitality occurred slowly, linearly
476 (asynchronously) and asymmetrically (when comparing daughter cells that remained together

after the MC). Thirdly, Yca1/Mca1, the main RCD player in *S. cerevisiae*, does not modulate the way vitality declines. Even though there are other RCD proteins aside from Yca1/Mca1 [56,57], we point out that that the pattern of cell death after the *top2* MC is better explained through ACD. Although we found intrinsic ROS production in a subset of the *top2* MC progeny and this finding has been considered a marker of RCD [41,58], we hypothesize that, in our case, ROS accumulation is another consequence of the steady decline of cell homeostasis. For instance, ROS might arise from either loss of nuclear genes encoding mitochondrial proteins or genes involved in eliminating ROS. Comparing with previous studies, the events that lead to death after the *top2* MC resemble those observed after prolonged G_2/M arrest in the *cdc13-1* mutant, which results in irreversible DNA damage at chromosome ends. In arrested *cdc13* cells, there are cell markers of RCD such as ROS production [59], although further biochemical assays or genetic manipulation suggest ACD rather than RCD [56]. In *cdc13-1*, because cells get blocked in G_2/M, there are no genetic imbalances prior to cell death. It was proposed that cell lysis, resulting from cell growth without cell division, was the ultimate cause of death, a hypothesis confirmed because sorbitol (an osmotic stabilizer) improved cell viability [56]. Although we also observed oversized cells one day after the *top2* MC (Fig 2A; 3A), cell lysis was a rare event and sorbitol did not improve cell viability (Fig 3). Therefore, we propose that the secondary ACD observed after the *top2* MC is the consequence of the steady decline of cell homeostasis resulting from loss of essential genes.

On the long-term genetic consequences of the *top2* mitotic catastrophe.

We have also compared the genomes of surviving diploids after 6h of Top2 inactivation. Even though we have not formally checked that all survivors came from a MC (i.e., they went through anaphase), the results shown in Figs 1-5, together with previous findings [20,35,36] lead us to conclude that most of these survivors likely came from a *top2* MC. Indeed, many of the observed chromosome variations and rearrangements can be best explained if cells go through anaphase in the absence of proper sister chromatid disjunction. Failure to decatenate sister chromatids results in DNA breaks that are repaired by RCOs or BIR. Previous studies also show that ABs get elevated in strains defective for sister chromatid decatenation such as *top2*, condensin mutants and *cdc14* [60–62].

One interpretation of the strong bias for T-LOH events relative to I-LOH events (76 terminal and 3 interstitial) is that DSBs are repaired primarily through BIR. In many previous studies, I-LOH represented a very significant fraction of the total LOH events. For example, in G_1-synchronized cells treated with ultraviolet light, we observed a 1:3 ratio between T-LOH and I-LOH [49]. Interstitial LOH requires both ends of the DSB to invade the other homolog during repair through homologous recombination, a condition difficult to fulfil in the DSBs generated by cytokinesis [18]. According to a previous study [60], the frequency of DSBs in *top2* mutants is higher for long chromosome arms than short chromosome arms. Our results are also consistent with this observation. Chromosome IV and XII right arms are the longest in the yeast genome and are overrepresented in the T-LOH events (normalizing for the size of the arm). An unusual feature of the T-LOH data is the rDNA is under-represented as a breakpoint in the cXIIr T-LOH events. It was previously shown, using an assay that detects loss of inserted marker within the rDNA, that *top2* strains have substantially elevated rates of mitotic recombination in the rDNA [63]. One possible explanation of this discrepancy is that DSBs within the rDNA may be repaired by single-strand annealing

between flanking copies of the rDNA genes [64], an event that could result in loss of an inserted marker without an interaction with the other homolog.

Another genetic alteration that is consistent with sister chromatid non-disjunction at the *top2* MC is the elevated presence of trisomies. A straightforward explanation for this is that the intertwining of sister chromatids in the *top2* strains often results in their co-segregation into one of the daughter cells. Although this type of non-disjunction would be expected to create equal numbers of monosomic and trisomic strains, it is possible that the monosomic strains have a competitive growth disadvantage and are, therefore, selected against. In *tel1 mec1* diploids, expected to enter anaphase with broken and/or underreplicated chromosomes, trisomies were five times more common than monosomies [65]. A similar bias towards trisomies was observed in *cdc14-1* diploids [66]; *cdc14* results in elevated levels of anaphase bridges because Cdc14 regulates condensin and Top2 actions in anaphase [67,68].

Lastly, the 100-fold enrichment in RUPD after the *top2* MC is also in agreement with models of genomic instability generated by sister chromatid non-disjunction. Two models are proposed for the generation of RUPD. One model involves two independent missegregation events occurring in successive divisions. In the other model, segregation of the chromosomes occurs in a manner similar to meiosis-I (Figs. S6 and S7). In wild-type cells, we demonstrated that the second model is correct [51]. From our data in the current study, we cannot distinguish between these models. The rate of a single non-disjunction event of chromosome V in a top2 mutant is very high, about 3×10^{-3}/division [34]. Thus, the likelihood of two independent non-disjunction events in a single division is $(3 \times 10^{-3})^2$ or 10^{-5} which is close to our observed rate of RUPD in the *top2-5* diploid. It is possible that both mechanisms contribute to the high rate of RUPD observed in the *top2-5* mutants. Another difference with

546 our earlier study [51] is the low frequency (18%) of sectors reflecting RUPD and RCO
547 recovered from the red/white Can^R sector assay. In our previous study, almost all of the
548 sectored colonies reflected RCOs or RUPD events. It is likely that the high levels of
549 aneuploidy observed in the *top2* mutants affects colony color by mechanisms unrelated to
550 RCO or RUPD events on chromosome V.

551 **CONCLUSIONS**

552 In this work, we have characterized the consequences for the progeny of depleting
553 yeast cells of Top2. We determined that the *top2* mitotic catastrophe leads to the sudden loss
554 of the capability to divide again. Nevertheless, restrictions for cell division are not a
555 consequence of immediate cell death as the progeny remain alive for several hours. In
556 addition, survivors of the *top2* mitotic catastrophe carry genomic footprints that point towards
557 sister chromatid non-disjunction and breakage of anaphase bridges as the source of the *top2*-
558 driven genome instability. Overall, the *top2*-mediated mitotic catastrophe is highly
559 deleterious for the cell progeny but it might also bring about highly unstable surviving clones.
560 Our results are of special interest to the field of Top2 catalytic inhibition as a promising
561 mechanism of action against cancer cells, especially those that have become resistant to anti-
562 Top2 poisons.

563

MATERIALS AND METHODS

Strain construction.

All strains used in this work are listed in Table S2. Gene deletions were achieved using standard PCR and transformation methods [36,69]. To obtain the transformation products, genomic DNA of the corresponding strain in the Euroscarf yeast haploid *MAT***a** knockout collection was used as the PCR template. Primers used in the PCR bind 100-400 bps upstream and downstream the deleted gene ORF (Table S3). Thus, the transformation product consisted in an amplicon containing either the *kanMX* or *URA3MX* selection markers flanked by 100-400 bps arms homologous to the targeting locus.

The *top2-5* isogenic homozygous diploid derivative was generated through a one-step marker-free transformation approach that takes advantage of the α-factor hypersensitivity in the haploid *MAT***a** *bar1*Δ genotype (a proof of concept is provided in Fig. S8). Briefly, haploid *MAT***a** *bar1*Δ strains were transformed with a PCR product obtained from a *MAT***α** haploid strain such that it only recombines with the *MAT* locus but not with the silent *HML/HMR* loci. We counterselected against the *MAT***a** genotype by spreading 5 µg α-factor on the Petri dish surface before spreading the transformed cells. Colonies resistant to α-factor were collected after 3-4 days at 25 ºC and checked by PCR for the *MAT***a**, *MAT***α** or *MAT***a**/*MAT***α** genotypes (Fig. S8). *MAT***a**/*MAT***α** diploids were further confirmed by sporulation capability and 2N DNA content by flow cytometry [70].

The *top2-5* heterozygous diploids FM1873 and MD684 were obtained by crossing of haploid strain *top2-5* derivatives of PSL2 and PSL5. These two strains are isogenic with W303-1A and YJM789, respectively, and have been engineered to select and visually detect

586 chromosome V rearrangements [47]. W303-1A and YJM789 differ by about 55,000 SNPs.
587 The PSL2 *top2-5* (FM1830) and PSL5 *top2-5* (FM1832) haploids were constructed by
588 transformation with a *top2-5:9xmyc:natNT2* product. This product was amplified by PCR
589 from a CH326 strain derivative in which the *top2-5* allele had been tagged at 3' with
590 sequences for 9 copies of the Myc epitope [71]. The heterozygous *top2-5/top2-5* diploid
591 FM1873 was obtained by crossing FM1830 and FM1832. After realizing that FM1873
592 already carried genome alterations at 25 ºC (3-4 copies of cXIV and cXIIr T-LOH), other
593 attempts to construct this diploid were undertaken. Previously, the FM1830 and FM1832
594 haploids were analysed and it was determined that FM1830 had 1-2 copies of cXIV. Thus,
595 FM1830 was backcrossed with W303 to cure the strain of genome alterations. One spore
596 (MD681) was identified that had the same genotype as FM1830 except that it had only one
597 copy of chromosome XIV. This strain was crossed to FM1832 to generate the diploid
598 MD684. Although these steps of construction were designed to generate a diploid that was
599 isogenic with FM1873 lacking the aneuploidy of XIV and the T-LOH event on cXIIr,
600 subsequent microarray analysis showed that MD684 still had three to four copies of XIV,
601 although the T-LOH event on cXIIr was absent.

602 Unless stated otherwise, all strains were grown overnight in air orbital incubators at
603 25 ºC in rich YPD media (1% w/v of yeast extract, 2% w/v peptone and 2% w/v dextrose)
604 before every experiment.

605

606 **Assays to assess clone survivability and capability of single cells to divide.**

A modified clonogenic assay was used to assess survivability of the progeny after the mitotic catastrophe. The purpose of this assay was to determine if at least one of the resulting cells in the progeny was still able to raise a new cell population. To this aim, 10^2 and 10^3 cells of an asynchronous logarithmic culture were spread onto a set of 14 YPD plates. These plates were then incubated for 0, 3, 6, 9, 12, 24 and 48 h at 37 ºC. After that, they were switched to 25 ºC to allow the growth of the survivors. Colonies were counted after 3-4 days and were normalized to the number of colonies grown without exposure to the restrictive temperature (0 h). By fixing the initial cell population on a solid medium, any clones that keep viability would give rise to a single macrocolony, irrespective of how many times the cell has divided and how many cells in the progeny are viable. Half-life values (t ½), the time in which the clone survival drops to 50%, were calculated adjusting the data to a four-parameter model using Graphpad Prism 7.

For the microcolony analysis, ~1.5 x 10^5 cells were spread onto a YPD (or YPD plus 1.2 M Sorbitol) plate to yield a density on the plate surface of around 25 cells per 10,000 μm^2. Defined positions on the plate were marked by piercing the surface with the needle of a Singer Sporeplay tetrad microdissector, using its 8 x 8 grid as a reference (12-16 fields in total). The plate was then transferred to a Leica LMD6000 direct microscope equipped with a 6.7x and 40x long-range objectives. The 6.7x was used to locate the marked fields and the 40x to take pictures of the cells in those fields (corresponding to 0 h, 25 ºC). Next, the plates were incubated at 37 ºC for 6 or 24 h before taking new pictures of the same fields. The procedure was repeated one more time after incubating the plate back at 25 ºC for 18-24 h. Finally, the same microcolonies in the corresponding three frames per field were identified by eye and categorized as indicated in the figure legends. The cell volume of the original mother

630 cell in all three frames was calculated assuming a perfect sphere and taking the cell diameter
631 for calculations.

632 For the single cell analysis by micromanipulation the different strains were streaked
633 on YPD Petri dishes. Unbudded cells were harvested with a Singer Sporeplay tetrad
634 microdissector. Just 12 cells were harvested per plate and arrayed along the A file stage grid
635 template in order to avoid prolonged incubations at 25º C. They were then incubated 6 h at 37
636 ºC and then observed under the microscope to count the number of cells that originated from
637 the initial cell. Next, each cell that had at least a new bud was subjected to a mild attempt to
638 separate the cell bodies using the needle and the vibration device. If successful, the largest
639 body remained in the A file, whereas the other body was transferred to the B file. Finally, the
640 plate was incubated 4 d at 25 ºC to search for survivors.

641 The segregation and morphology of the histone-labelled nucleus (H2A-GFP) was
642 analyzed by wide-field fluorescence videomicroscopy. An asynchronous culture was
643 concentrated by centrifugation to OD_{660} of 3 and spread onto YPD agar 90 mm Petri dishes.
644 Patches were made from this plate and mounted in a microscope slide. They were incubated
645 at 37 ºC for 24 h in high humidity chambers to avoid the patch to dry. The same fields were
646 photomicrographed at 0, 6 and 24 h. For each time point, a series of z-focal plane images (10
647 planes, 0.6 µm depth) were collected on a Leica DMI6000, using a 63x/1.30 immersion
648 objective and an ultrasensitive DFC 350 digital camera, and processed with the AF6000
649 software (Leica).

650

651 **Assays to assess cell vitality and cell death.**

All the colorimetric and fluorometric assays to assess metabolic competence, ROS production, and plasma membrane permeability were carried out in asynchronous logarithmic cultures grown overnight at 25 ºC, adjusting the OD_{600} to 0.2 and incubated them for 24 h at 37 ºC. Samples were taken at 0, 4 and 24 h, unless stated otherwise, and directly observed under the microscope. Fluorescence microscopy was used instead of flow cytometry because strains were already fluorescent for H2A-GFP. ROS were visualized with 10 µg/ml of 2′,7′-dichlorofluorescin diacetate (DCFH-DA; Sigma-Aldrich; D6883); and 3 µg/ml PI (Fluka; #81845) was used to count dead cells. Both dyes were directly mixed with a 200 µl aliquot of the culture and incubated 15 min at 37 ºC in the dark. Cell bodies were considered ROS positive when the cytoplasm stained green in the absence of staining for PI. FUN® 1 (Invitrogen; F7030) staining was done washing 200 µl of each sample with water containing 2% D-(+)-glucose and 10 mM Na-HEPES, pH 7.2, resuspending the cells in the same buffer with 10 µM FUN® 1 and incubating 30 min at 37 ºC in the dark. For MB (Sigma-Aldrich; M9140) staining, 1 µl of each sample was mixed with 1 µl of a 0.04% w/v MB solution in water onto a microscope slide and directly visualized (bright field).

Analysis of genomic rearrangements using microarrays

Two similar protocols were used to expose heterozygous diploids to the *top2*-mediated mitotic catastrophe. For both protocols, cells were grown in YPD to an optical density of 0.5-1. For one set of experiments (marked as E1 in the tables in the text), the cells were struck for single colonies on plates containing solid YPD medium, incubated for 6 hours at 37 ºC, then incubated at room temperature until colonies had formed. For the second protocol, the cells grown at room temperature were harvested by centrifugation, and

675 resuspended in 37 ºC liquid medium, followed by incubation for 6 hours at 37 ºC. Following
676 this incubation, they were struck on YPD plates and incubated at room temperature until
677 colonies were formed. For both protocols, the control cells were struck to room temperature
678 YPD plates without incubating them at 37 ºC. In experiments to detect sectored colonies, the
679 YPD medium was replaced with solid omission medium lacking arginine and containing 120
680 µg/ml canavanine [48].

681 We detected LOH events, aneuploidy and UPD using SNP-specific microarrays
682 similar to those used by [72]. The details of this procedure have been described before
683 [45,46]. In brief, for most experiments, genomic DNA was obtained from single-colony
684 isolates of experimental samples (incubated for six hours at 37 ºC) that was labeled with Cy5-
685 dUTP. Two different types of microarray-control DNA were used and labelled with Cy3-
686 dUTP. For some experiments, we used DNA purified from the FM1873 culture before
687 exposure to 37 ºC. In other experiments, we used DNA from the *TOP2/TOP2* isogenic strain
688 JSC24 [49]. Following labeling of the samples, the experimental and microarray-control
689 DNA samples were mixed and hybridized to the microarrays [45]. The microarrays were then
690 scanned at wavelengths 532 and 635 nm with a GenePix scanner, and analyzed by GenePix
691 Pro software. Hybridization signals for Cy5 and Cy3 were normalized over the array to a
692 value of 1. Additional steps of normalization are described in [45]. Following normalization,
693 the ratio of hybridization of the experimental samples to the control samples for individual
694 SNPs was 1 if the experimental strain was heterozygous. In analysis of single-colony isolates,
695 whole-genome arrays were used (Gene Expression Omnibus [GEO] #GPL20144). For
696 analysis of sectored colonies, we used microarrays specific for the right arm of V, and
697 chromosomes I, III, and VIII (GEO #GPL21274).

698

699 **AKNOWLEDGEMENTS**

700 We thank other members of both labs and Kerry Bloom for fruitful discussions and
701 help. We also thank Jessel Ayra-Plasencia, Nayra Cabrera-Quintero and Annika Lange for
702 technical help in some of the experiments that required micromanipulation and microcolony
703 counting. We thank Yang Sui for help with Figures S6 and S7.

704 The research was supported by the following grant funders: NIH (R35 GM118020)
705 and Army Research Office (SPS #200531) to Thomas D Petes; Agencia Española de
706 Investigación (BFU2015-63902-R and BFU2017-83954-R) to Félix Machín. Cristina Ramos-
707 Pérez was a recipient of a predoctoral fellowship by the Agencia Canaria de Investigación,
708 Innovación y Sociedad de la Información (ACIISI; TESIS20120109). F.M.'s grants and C.R-
709 P.'s fellowship were co-funded by the European Commission's European Regional
710 Development Fund (ERDF).

711

712 **REFERENCES**

713 1. Hayashi MT, Karlseder J. DNA damage associated with mitosis and cytokinesis
714 failure. Oncogene. 2013;32: 4593–601. doi:10.1038/onc.2012.615

715 2. Portugal J, Mansilla S, Bataller M. Mechanisms of drug-induced mitotic catastrophe in
716 cancer cells. Curr Pharm Des. 2010;16: 69–78. doi:10.2174/138161210789941801

717 3. Galluzzi L, Vitale I, Abrams JM, Alnemri ES, Baehrecke EH, Blagosklonny M V, et
718 al. Molecular definitions of cell death subroutines: recommendations of the
719 Nomenclature Committee on Cell Death 2012. Cell Death Differ. 2012;19: 107–120.
720 doi:10.1038/cdd.2011.96

721 4. Galluzzi L, Bravo-San Pedro JM, Vitale I, Aaronson S a, Abrams JM, Adam D, et al.
722 Essential versus accessory aspects of cell death: recommendations of the NCCD 2015.
723 Cell Death Differ. 2014; 58–73. doi:10.1038/cdd.2014.137

724 5. Chan K-S, Koh C-G, Li H-Y. Mitosis-targeted anti-cancer therapies: where they stand.
725 Cell Death Dis. 2012;3: e411. doi:10.1038/cddis.2012.148

726 6. Galluzzi L, Vitale I, Vacchelli E, Kroemer G. Cell Death Signaling and Anticancer
727 Therapy. Front Oncol. 2011;1: 1–18. doi:10.3389/fonc.2011.00005

728 7. Ishikawa K, Ishii H, Saito T. DNA damage-dependent cell cycle checkpoints and
729 genomic stability. DNA Cell Biol. 2006;25: 406–11. doi:10.1089/dna.2006.25.406

730 8. Bieging KT, Mello SS, Attardi LD. Unravelling mechanisms of p53-mediated tumour
731 suppression. Nat Rev Cancer. Nature Publishing Group; 2014;14: 359–70.
732 doi:10.1038/nrc3711

733 9. Abraham RT. Cell cycle checkpoint signalling through the ATM and ATR kinases.
734 Genes Dev. 2001;15: 2177–2196. doi:10.1101/gad.914401.DNA

735 10. Duch A, Nadal E De, Posas F. The p38 and Hog1 SAPKs control cell cycle
736 progression in response to environmental stresses. FEBS Lett. Federation of European
737 Biochemical Societies; 2012;586: 2925–2931. doi:10.1016/j.febslet.2012.07.034

738 11. Brown A, Geiger H. Chromosome integrity checkpoints in stem and progenitor cells:
739 transitions upon differentiation, pathogenesis, and aging. Cell Mol Life Sci. Springer
740 International Publishing; 2018;75: 3771–3779. doi:10.1007/s00018-018-2891-z

741 12. Dashzeveg N, Yoshida K. Crosstalk between tumor suppressors p53 and PKCδ:
742 Execution of the intrinsic apoptotic pathways. Cancer Lett. Elsevier Ireland Ltd;
743 2016;377: 158–163. doi:10.1016/j.canlet.2016.04.032

744 13. Fulda S, Debatin KM. Extrinsic versus intrinsic apoptosis pathways in anticancer
745 chemotherapy. Oncogene. 2006;25: 4798–4811. doi:10.1038/sj.onc.1209608

746 14. Vitale I, Galluzzi L, Castedo M, Kroemer G. Mitotic catastrophe: a mechanism for
747 avoiding genomic instability. Nat Rev Mol Cell Biol. 2011;12: 385–92.
748 doi:10.1038/nrm3115

749 15. Hoffelder DR, Luo L, Burke NA, Watkins SC, Gollin SM, Saunders WS. Resolution
750 of anaphase bridges in cancer cells. Chromosoma. 2004;112: 389–97.
751 doi:10.1007/s00412-004-0284-6

16. Ganem NJ, Pellman D. Linking abnormal mitosis to the acquisition of DNA damage. J Cell Biol. 2012;199: 871–881. doi:10.1083/jcb.201210040

17. Quevedo O, García-Luis J, Matos-Perdomo E, Aragón L, Machín F. Nondisjunction of a single chromosome leads to breakage and activation of DNA damage checkpoint in g2. Lacefield S, editor. PLoS Genet. Public Library of Science; 2012;8: e1002509. doi:10.1371/journal.pgen.1002509

18. Machín F, Quevedo O, Ramos-Pérez C, García-Luis J. Cdc14 phosphatase: warning, no delay allowed for chromosome segregation! Curr Genet. Springer Berlin Heidelberg; 2016;62: 7–13. doi:10.1007/s00294-015-0502-1

19. Uemura T, Tanagida M. Mitotic spindle pulls but fails to separate chromosomes in type II DNA topoisomerase mutants: uncoordinated mitosis. EMBO J. 1986;5: 1003–10.

20. Holm C, Goto T, Wang JC, Botstein D. DNA topoisomerase II is required at the time of mitosis in yeast. Cell. 1985;41: 553–63.

21. Gorbsky GJ. Cell cycle progression and chromosome segregation in mammalian cells cultured in the presence of the topoisomerase II inhibitors ICRF-187 [(+)-1,2-bis(3,5-dioxopiperazinyl-1-yl)propane; ADR-529] and ICRF-159 (Razoxane). Cancer Res. 1994;54: 1042–8.

22. Damelin M, Sun YE, Sodja VB, Bestor TH. Decatenation checkpoint deficiency in stem and progenitor cells. Cancer Cell. 2005;8: 479–484. doi:10.1016/j.ccr.2005.11.004

23. Damelin M, Bestor TH. The decatenation checkpoint. Br J Cancer. 2007;96: 201–205. doi:10.1038/sj.bjc.6603537

24. Bower JJ, Karaca GF, Zhou Y, Simpson D a, Cordeiro-Stone M, Kaufmann WK. Topoisomerase IIalpha maintains genomic stability through decatenation G(2) checkpoint signaling. Oncogene. Nature Publishing Group; 2010;29: 4787–4799. doi:10.1038/onc.2010.232

25. Downes CS, Clarke DJ, Mullinger AM, Giménez-Abián JF, Creighton AM, Johnson RT. A topoisomerase II-dependent G2 cycle checkpoint in mammalian cells. Nature. 1994;372: 467–470. doi:10.1038/372467a0

26. Giménez-Abián JF, Clarke DJ, Giménez-Martín G, Weingartner M, Giménez-Abián MI, Carballo J a, et al. DNA catenations that link sister chromatids until the onset of anaphase are maintained by a checkpoint mechanism. Eur J Cell Biol. 2002;81: 9–16.

27. Franchitto A, Oshima J, Pichierri P. The G2-phase decatenation checkpoint is defective in Werner syndrome cells. Cancer Res. 2003;63: 3289–3295.

28. Nakagawa T, Hayashita Y, Maeno K, Masuda A, Sugito N, Osada H, et al. Identification of decatenation G2 checkpoint impairment independently of DNA damage G2 checkpoint in human lung cancer cell lines. Cancer Res. 2004;64: 4826–4832. doi:10.1158/0008-5472.CAN-04-0871

29. Brooks K, Chia KM, Spoerri L, Mukhopadhyay P, Wigan M, Stark M, et al. Defective decatenation checkpoint function is a common feature of melanoma. J Invest Dermatol. Nature Publishing Group; 2014;134: 150–8. doi:10.1038/jid.2013.264

30. Jain CK, Roychoudhury S, Majumder HK. Selective killing of G2decatenation checkpoint defective colon cancer cells by catalytic topoisomerase II inhibitor. Biochim Biophys Acta - Mol Cell Res. Elsevier B.V.; 2015;1853: 1195–1204. doi:10.1016/j.bbamcr.2015.02.021

31. Nitiss JL. Targeting DNA topoisomerase II in cancer chemotherapy. Nat Rev Cancer. 2009;9: 338–50. doi:10.1038/nrc2607

32. Holohan C, Van Schaeybroeck S, Longley DB, Johnston PG. Cancer drug resistance: an evolving paradigm. Nat Rev Cancer. 2013;13: 714–26. doi:10.1038/nrc3599

33. DiNardo S, Voelkel K, Sternglanz R. DNA topoisomerase II mutant of Saccharomyces cerevisiae: topoisomerase II is required for segregation of daughter molecules at the termination of DNA replication. Proc Natl Acad Sci U S A. 1984;81: 2616–20.

34. Holm C, Stearns T, Botstein D. DNA topoisomerase II must act at mitosis to prevent nondisjunction and chromosome breakage. Mol Cell Biol. 1989;9: 159–68.

35. Baxter J, Diffley JFX. Topoisomerase II inactivation prevents the completion of DNA replication in budding yeast. Mol Cell. 2008;30: 790–802. doi:10.1016/j.molcel.2008.04.019

36. Ramos-Pérez C, Ayra-Plasencia J, Matos-Perdomo E, Lisby M, Brown GW, Machín F. Genome-Scale Genetic Interactions and Cell Imaging Confirm Cytokinesis as Deleterious to Transient Topoisomerase II Deficiency in Saccharomyces cerevisiae. G3 (Bethesda). 2017;7: 3379–3391. doi:10.1534/g3.117.300104

37. Carmona-Gutierrez D, Bauer MA, Zimmermann A, Aguilera A, Austriaco N, Ayscough K, et al. Guidelines and recommendations on yeast cell death nomenclature. Microb Cell. 2018;5: 4–31. doi:10.15698/mic2018.01.607

38. Klein HL, Bačinskaja G, Che J, Cheblal A, Elango R, Epshtein A, et al. Guidelines for DNA recombination and repair studies: Cellular assays of DNA repair pathways. Microb Cell. 2019;6: 1–64. doi:10.15698/mic2019.01.664

39. Kucsera J, Yarita K, Takeo K. Simple detection method for distinguishing dead and living yeast colonies. J Microbiol Methods. 2000;41: 19–21.

40. Millard PJ, Roth BL, Thi HPT, Yue ST, Haugland RP. Development of the FUN-1 family of fluorescent probes for vacuole labeling and viability testing of yeasts. Appl Environ Microbiol. 1997;63: 2897–2905.

41. Madeo F, Fröhlich E, Ligr M, Grey M, Sigrist SJ, Wolf DH, et al. Oxygen stress: A regulator of apoptosis in yeast. J Cell Biol. 1999;145: 757–767. doi:10.1083/jcb.145.4.757

42. Carmona-Gutierrez D, Eisenberg T, Büttner S, Meisinger C, Kroemer G, Madeo F. Apoptosis in yeast: triggers, pathways, subroutines. Cell Death Differ. 2010;17: 763–73. doi:10.1038/cdd.2009.219

43. Madeo F, Herker E, Maldener C, Wissing S, Lächelt S, Herlan M, et al. A caspase-related protease regulates apoptosis in yeast. Mol Cell. 2002;9: 911–7.

44. Mitsui K, Nakagawa D, Nakamura M, Okamoto T, Tsurugi K. Valproic acid induces apoptosis dependent of Yca1p at concentrations that mildly affect the proliferation of yeast. FEBS Lett. 2005;579: 723–727. doi:10.1016/j.febslet.2004.12.051

836 45. St. Charles J, Hazkani-Covo E, Yin Y, Andersen SL, Dietrich FS, Greenwell PW, et al.
837 High-resolution genome-wide analysis of irradiated (UV and γ-Rays) diploid yeast
838 cells reveals a high frequency of genomic loss of heterozygosity (LOH) events.
839 Genetics. 2012;190: 1267–1284. doi:10.1534/genetics.111.137927

840 46. St. Charles J, Petes TD. High-Resolution Mapping of Spontaneous Mitotic
841 Recombination Hotspots on the 1.1 Mb Arm of Yeast Chromosome IV. PLoS Genet.
842 2013;9. doi:10.1371/journal.pgen.1003434

843 47. Lee PS, Greenwell PW, Dominska M, Gawel M, Hamilton M, Petes TD. A fine-
844 structure map of spontaneous mitotic crossovers in the yeast Saccharomyces
845 cerevisiae. PLoS Genet. 2009;5: e1000410. doi:10.1371/journal.pgen.1000410

846 48. Barbera MA, Petes TD. Selection and analysis of spontaneous reciprocal mitotic cross-
847 overs in Saccharomyces cerevisiae. Proc Natl Acad Sci U S A. 2006;103: 12819–24.
848 doi:10.1073/pnas.0605778103

849 49. Yin Y, Petes TD. Genome-Wide High-Resolution Mapping of UV-Induced Mitotic
850 Recombination Events in Saccharomyces cerevisiae. PLoS Genet. 2013;9.
851 doi:10.1371/journal.pgen.1003894

852 50. Jannatipour M, Liu YX, Nitiss JL. The top2-5 mutant of yeast topoisomerase II
853 encodes an enzyme resistant to etoposide and amsacrine. J Biol Chem. 1993;268:
854 18586–92.

855 51. Andersen SL, Petes TD. Reciprocal uniparental disomy in yeast. Proc Natl Acad Sci.
856 2012;109: 9947–9952. doi:10.1073/pnas.1207736109

857 52. Burgess A, Rasouli M, Rogers S. Stressing Mitosis to Death. Front Oncol. 2014;4: 1–
858 7. doi:10.3389/fonc.2014.00140

859 53. Andrews CA, Vas AC, Meier B, Giménez-Abián JF, Díaz-Martínez LA, Green J, et al.
860 A mitotic topoisomerase II checkpoint in budding yeast is required for genome
861 stability but acts independently of Pds1/securin. Genes Dev. 2006;20: 1162–74.
862 doi:10.1101/gad.1367206

863 54. Endo K, Mizuguchi M, Harata A, Itoh G, Tanaka K. Nocodazole induces mitotic cell
864 death with apoptotic-like features in Saccharomyces cerevisiae. FEBS Lett. Federation
865 of European Biochemical Societies; 2010;584: 2387–92.
866 doi:10.1016/j.febslet.2010.04.029

867 55. Zierhut C, Diffley JFX. Break dosage, cell cycle stage and DNA replication influence
868 DNA double strand break response. EMBO J. 2008;27: 1875–85.
869 doi:10.1038/emboj.2008.111

870 56. Wysocki R, Kron SJ. Yeast cell death during DNA damage arrest is independent of
871 caspase or reactive oxygen species. J Cell Biol. 2004;166: 311–6.
872 doi:10.1083/jcb.200405016

873 57. Váchová L, Palková Z. Caspases in yeast apoptosis-like death: facts and artefacts.
874 FEMS Yeast Res. 2007;7: 12–21. doi:10.1111/j.1567-1364.2006.00137.x

875 58. Perrone GG, Tan S-X, Dawes IW. Reactive oxygen species and yeast apoptosis.
876 Biochim Biophys Acta. 2008;1783: 1354–68. doi:10.1016/j.bbamcr.2008.01.023

877 59. Qi H, Li TK, Kuo D, Nur-E-Kamal A, Liu LF. Inactivation of Cdc13p triggers MEC1-

878 dependent apoptotic signals in yeast. J Biol Chem. 2003;278: 15136–15141.
879 doi:10.1074/jbc.M212808200

880 60. Spell RM, Holm C. Nature and distribution of chromosomal intertwinings in
881 Saccharomyces cerevisiae. Mol Cell Biol. 1994;14: 1465–76.

882 61. Freeman L, Aragon-Alcaide L, Strunnikov A. The condensin complex governs
883 chromosome condensation and mitotic transmission of rDNA. J Cell Biol. 2000;149:
884 811–24.

885 62. Machín F, Torres-Rosell J, Jarmuz A, Aragón L. Spindle-independent condensation-
886 mediated segregation of yeast ribosomal DNA in late anaphase. J Cell Biol. 2005;168:
887 209–19. doi:10.1083/jcb.200408087

888 63. Christman MF, Dietrich FS, Fink GR. Mitotic recombination in the rDNA of S.
889 cerevisiae is suppressed by the combined action of DNA topoisomerases I and II. Cell.
890 1988;55: 413–25.

891 64. Ozenberger BA, Roeder GS. A unique pathway of double-strand break repair operates
892 in tandemly repeated genes. Mol Cell Biol. 1991;11: 1222–31.
893 doi:10.1128/mcb.11.3.1222

894 65. McCulley JL, Petes TD. Chromosome rearrangements and aneuploidy in yeast strains
895 lacking both Tel1p and Mec1p reflect deficiencies in two different mechanisms. Proc
896 Natl Acad Sci U S A. 2010;107: 11465–70. doi:10.1073/pnas.1006281107

897 66. Quevedo O, Ramos-Perez C, Petes TD, Machin F. The Transient Inactivation of the
898 Master Cell Cycle Phosphatase Cdc14 Causes Genomic Instability in Diploid Cells of
899 Saccharomyces cerevisiae. Genetics. 2015;200: 755–769.
900 doi:10.1534/genetics.115.177626

901 67. D'Amours D, Stegmeier F, Amon A. Cdc14 and condensin control the dissolution of
902 cohesin-independent chromosome linkages at repeated DNA. Cell. 2004;117: 455–69.

903 68. Sullivan M, Higuchi T, Katis VL, Uhlmann F. Cdc14 phosphatase induces rDNA
904 condensation and resolves cohesin-independent cohesion during budding yeast
905 anaphase. Cell. 2004;117: 471–82.

906 69. Smith JS, Burke DJ. Yeast Genetics: Methods and Protocols. Smith JS, Burke DJ,
907 editors. New York, NY: Springer New York; 2014. doi:10.1007/978-1-4939-1363-3

908 70. García-Luis J, Machín F. Mus81-Mms4 and Yen1 resolve a novel anaphase bridge
909 formed by noncanonical Holliday junctions. Nat Commun. 2014;5: 5652.
910 doi:10.1038/ncomms6652

911 71. Janke C, Magiera MM, Rathfelder N, Taxis C, Reber S, Maekawa H, et al. A versatile
912 toolbox for PCR-based tagging of yeast genes: new fluorescent proteins, more markers
913 and promoter substitution cassettes. Yeast. 2004;21: 947–62. doi:10.1002/yea.1142

914 72. Gresham D, Curry B, Ward A, Gordon DB, Brizuela L, Kruglyak L, et al. Optimized
915 detection of sequence variation in heterozygous genomes using DNA microarrays with
916 isothermal-melting probes. Proc Natl Acad Sci. 2010;107: 1482–1487.
917 doi:10.1073/pnas.0913883107

918

919

920 **Table 1. Genomic changes in single-colony isolates of FM1873 and MD684.**

Strain name[1]	Genomic alterations[2]
FM1873-01 (E1)	T-LOH (966 kb on IV), Tri (V), Partial UPD (VII), Tri (X)
FM1873-04 (E1)	T-LOH (471 kb on IV), UPD (VIII), 3 T-LOH events (XIII, breakpoints at 450 kb, 777 kb, and 864 kb)
FM1873-11 (E1)	UPD (IV), Tri (VIII), Mon (IX), Tri (X), Partial Tri (XV), UPD (XVI)
FM1873-1 (E2)	UPD (IV), Tri (XV)
FM1873-2 (E2)	T-LOH (790 kb on IV)
FM1873-3 (E2)	T-LOH (790 kb on IV)
FM1873-4 (E2)	T-LOH (671 kb on IV), Tri (V), Tri (VII), T-LOH (1002 kb on XV)
FM1873-5 (E2)	T-LOH (755 kb on IV), T-LOH (450 kb on XIII)
FM1873-11X (E2)	T-LOH (958 kb on IV), Tri (VII)
FM1873-12 (E2)	Tri (VIII)
FM1873-13 (E2)	T-LOH (668 kb on IV), Tri (V), T-LOH (1002 kb on XV)
FM1873-14 (E2)	T-LOH (1018 kb on IV)
FM1873-15 (E2)	T-LOH (483 kb on IV)
FM1873-C1 (C1)	No additional alterations
FM1873-C2 (C1)	No additional alterations
FM1873-C3 (C1)	Two T-LOH events (485 kb and 820 kb on IV)
FM1873-C4 (C1)	T-LOH (470 kb on IV), T-LOH (856 kb on XIII), T-LOH (216 kb on XIV)
FM1873-1c (C2)	Two T-LOH (456 kb and 1440 kb on IV); T-LOH (385 kb on VII), T-LOH (400 kb on XIV)
FM1873-2c (C2)	Two T-LOH (957 kb and 1440 kb on IV)
FM1873-3c (C2)	T-LOH (935 kb on IV), Tri (V)
FM1873-4c (C2)	T-LOH (858 kb on IV)

FM1873-5c (C2)	Tri and T-LOH (1270 kb on IV), Tri (V), Partial Tri (XIII)
FM1873-11c (C2)	T-LOH (1017 kb on IV), Tri (VIII), Tri (XV)
FM1873-12c (C2)	T-LOH (1004 kb on IV), Tri (X), Tri (XV)
FM1873-13c (C2)	T-LOH (1017 kb on IV), Tri (VIII)
FM1873-14c (C2)	Two T-LOH events (889 kb and 1221 kb on IV)
FM1873-15c (C2)	I-LOH (1354-1357 kb on IV), T-LOH (1474 kb on IV), Tri (V), UPD (VIII)
MD684.1.1 (E1)	T-LOH (596 kb on IV), T-LOH (7.5 kb on XI), T-LOH (430 kb on XII)
MD684.1.2 (E1)	T-LOH (808 kb on IV), Tri (VIII)
MD684.1.3 (E1)	T-LOH (1002 kb on IV), T-LOH (165 kb on XII)
MD684.1.4 (E1)	T-LOH (458 kb on IV), Tri (XV)
MD684.1.5 (E1)	T-LOH (1065 on IV), Tri (VIII), Two T-LOH (253 kb and 446 kb on XII)
MD684.1.6 (E2)	Partial Tri (II)
MD684.1.7 (E2)	T-LOH (1028 kb on IV), T-LOH (29 kb on VII), T-LOH (175 kb on XII)
MD684.1.8 (E2)	Three T-LOH (921 kb, 1050 kb and 1070 kb on IV), T-LOH (538 kb on V), T-LOH (450 kb on XII)
MD684.1.9 (E2)	Partial monosomy (I), Tri and T-LOH (486 kb on IV)
MD684.1.10 (E2)	Two T-LOH (661 kb and 963 kb on IV), Tri and T-LOH (626 kb on XV)
MD684 C1.1 (C1)	I-LOH (747-760 kb on IV), T-LOH (840 kb on IV), T-LOH (176 kb on XII)
MD684 C1.2 (C1)	T-LOH (458 kb on IV), T-LOH (447 kb on XII)
MD684 C1.3 (C1)	Two T-LOH (893 kb and 1472 kb on IV), Tri (V), T-LOH (170 kb on XII)
MD684 C1.4 (C1)	Tri (I), T-LOH (920 kb on IV)
MD684 C1.5 (C1)	T-LOH (527 kb on IV), Tri (XII)

MD684 C1.6 (C2)	Two T-LOH (680 kb and 1050 kb on IV), T-LOH (760 kb on VII), T-LOH (175 kb on XII)
MD684 C1.7 (C2)	T-LOH (1008 on IV), I-LOH (215-228 kb on XII), T-LOH (277 kb on XII), Partial Tri (XVI)
MD684 C1.8 (C2)	T-LOH (842 kb on IV), T-LOH (657 kb on XV)
MD684 C1.9 (C2)	T-LOH (1028 kb on IV)

[1] Parentheses after the strain name indicate whether the strain was experimental (E, incubated for six hours at 37 ºC) or control (C, not incubated at 37 ºC). E1 and C1 indicates that the 37 ºC incubation was done on plates; in E2 and C2 experiments, the 37 ºC incubations were done in liquid.

[2] Strains derived from FM1873 (both experimental (incubated at 37 ºC for six hours) and control (not incubated at 37 ºC) strains had three to four copies of chromosome XIV and a terminal LOH event on the right arm of chromosome XII (breakpoint at 236 kb). These alterations, therefore, are not listed in the FM1873 strains. The MD684 strain also had three to four copies of chromosome XIV in isolates, and this alteration is not shown in the table. Code: T-LOH (terminal LOH event), I-LOH (interstitial LOH event), Tri (trisomy), Mon (monosomy), UPD (uniparental disomy).

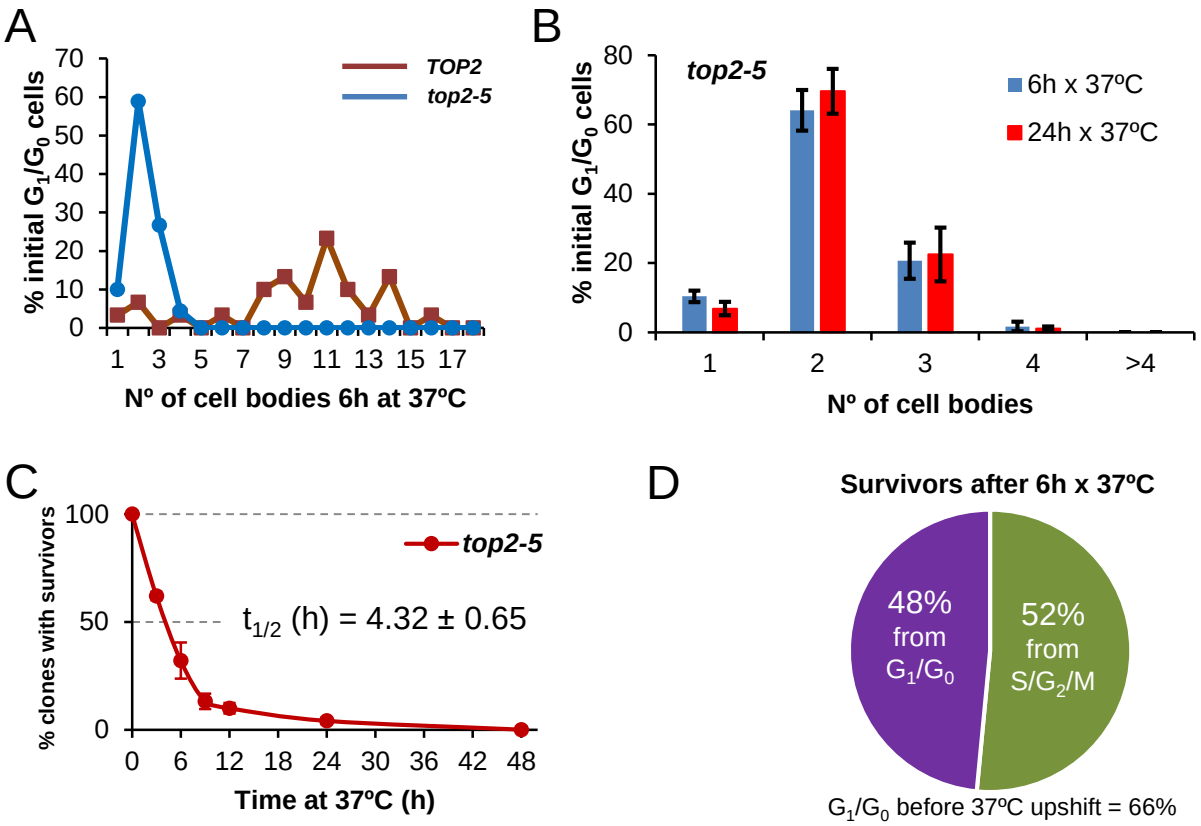

Figure 1. Most daughter cells coming from a Top2-mediated mitotic catastrophe are unable to divide again (I). (**A**) Haploid *TOP2* (WT) or *top2-5* cells were grown at 25 ºC and spread on YPD agar plates. Unbudded cells (G_1/G_0) were identified and photographed again after 6 h at 37 ºC. Number of cell bodies (buds) coming from these G_1/G_0 cells were then counted and plotted as indicated. (**B**) The same analysis as in panel A but including data coming from independent experiments as well as after 24 h incubation at 37 ºC (mean ± s.e.m., n=3). (**C**) Time course of clonogenic survivability. Asynchronous *top2-5* cultures growing at 25 ºC were spread onto several YPD plates. The plates were incubated at 37 ºC for different periods before transferring them 25 ºC. Four days after the initial plating, visible colonies (macrocolonies) were counted and normalized to a control plate which was never incubated at 37 ºC (0h). (**D**) Analysis of the origin of macrocolonies after the 6 h x 37 ºC regime as determined after microscanning plates at the time of seeding (N=33 macrocolonies; 2:1 unbudded:budded ratio at seeding).

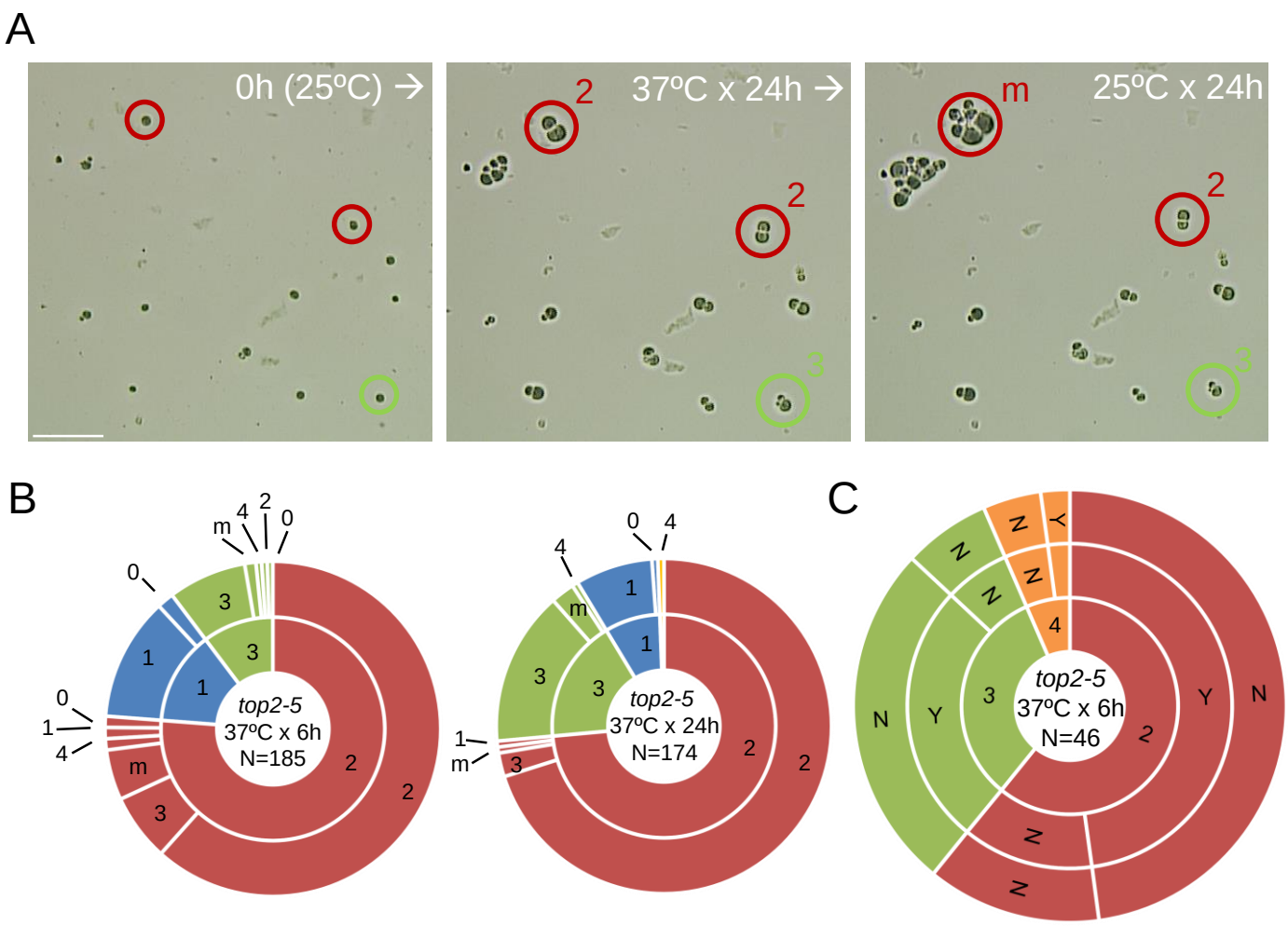

Figure 2. Most daughter cells coming from a Top2-mediated mitotic catastrophe are unable to divide again (II). Haploid *top2-5* cells were grown and spread at high cell density on two Petri dishes. At the time of seeding, 0h (25 ºC), several fields were photomicrographed before incubating the plates at 37 ºC during either 6 h or 24 h. After the 37 ºC incubation, the same fields were localized, photomicrographed again, and further incubated 16-24 h at 25 ºC. (**A**) An example of a microscope field of a 37 ºC x 24 h experiment. Three representative unbudded cells at 0h (25 ºC) are highlighted. In red, two cells that budded just once during the 37 ºC x 24 h incubation ("2" cell bodies); one of them able to re-bud again a few times after the 25 ºC downshift ("m") and the second one that remained stuck as "2". In green, a cell that reached "3" bodies at 37º C and remained so after the final 25 ºC x 24 h incubation. Scale bar corresponds to 50 µm. (**B**) Analysis of how far the *top2-5* progeny can go after the mitotic catastrophe, based on the microcolony approach shown in panel A. Only unbudded (G_1/G_0) cells at 0h (25 ºC) were considered. The inner circle in the sunburst chart depicts the number of cell bodies after the 37 ºC incubation. The outer circle depicts the situation after the final 25 ºC incubations (16 h for the 6h x 37 ºC regime and 24 h for the 6h x 37 ºC regime). On the left are results from a 37 ºC x 6 h regime; on the right are results from a 37 ºC x 24 h regime. Numbers point to the number of cell bodies; "m" means microcolonies of 5 or more bodies. (**C**) Capability of the *top2-5* progeny to split apart and relationship with overall survivability. Unbudded cells were micromanipulated and arranged at defined plate positions before incubating then 6 h at 37 ºC. Then, those cells able to re-bud at least once were subjected to an attempt to physically separate the cell bodies. The inner circle in the sunburst depicts the number of cell bodies after the 6 h at 37 ºC incubation. The middle circle depicts the result of the separation attempt ("Y" or "N", successful or unsuccessful, respectively). The outer circle indicates if any of the bodies was able to raise a macrocolony (Yes or No) after 4 d incubation at 25 ºC. N, number of original unbudded cells which were followed. Blue sectors, G_1/G_0 cells that remained unbudded during the 37 ºC incubations; red sectors; cells that budded once at 37 ºC; green sectors, cells that reached 3 bodies at 37 ºC; orange sectors, cells that reached 4 or more bodies at 37 ºC.

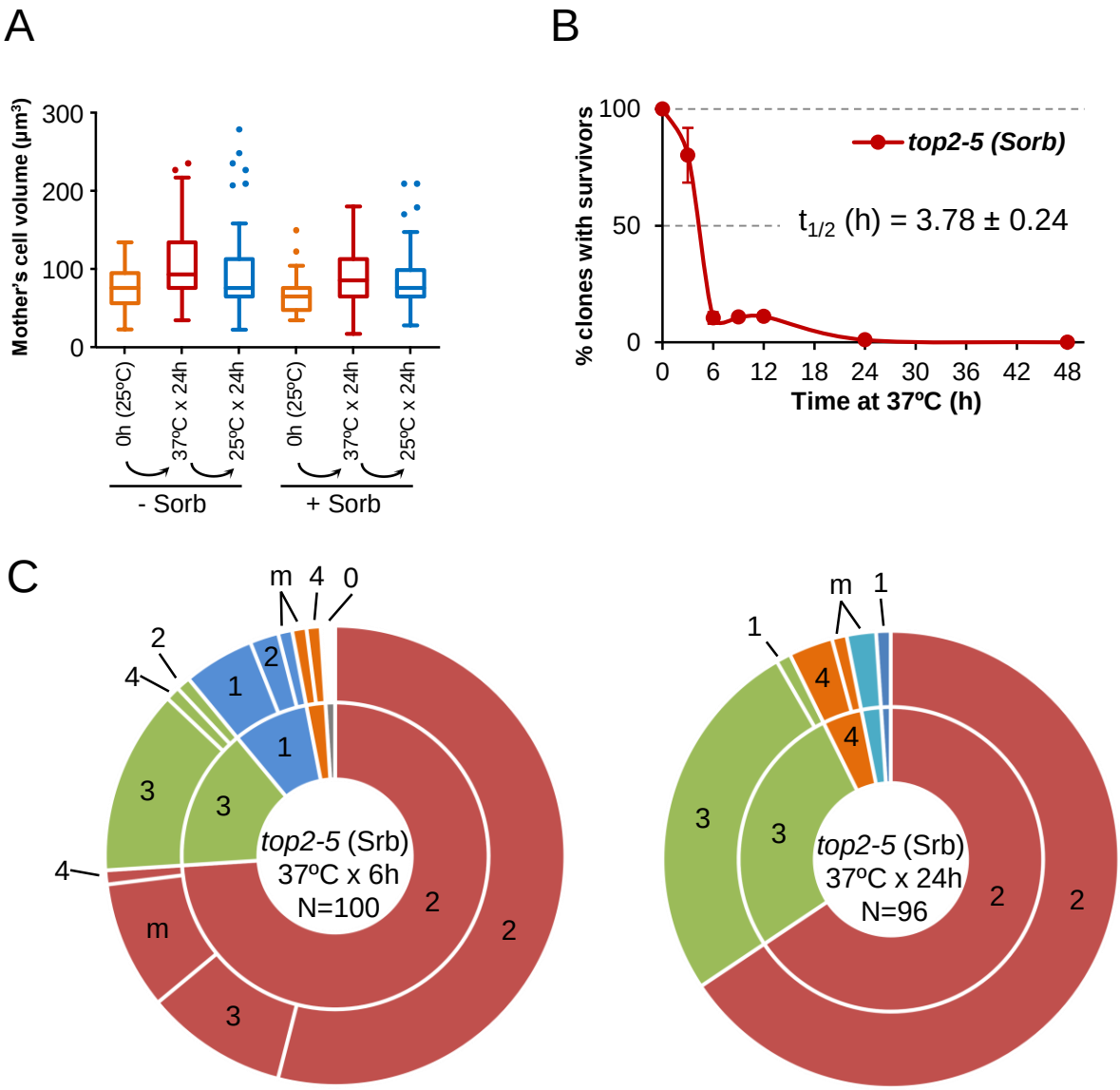

Figure 3. Osmotic stress plays no role in the inability to divide of the *top2-5* progeny. (**A**) Progression of the size (volume) of the original G_1/G_0 cells (mother) after the *top2-5* mitotic catastrophe with and without the osmotic stabilizer Sorbitol (Sorb, 1.2 M). (B) Time course of clonogenic survivability in the presence of 1.2 M Sorbitol. The experiment was conducted as in 1C. (**C**) Sunbursts of microcolony analyses in the presence of 1.2 M Sorbitol (Srb) at the 6 h and 24 h x 37 ºC regimes. Interpretation as in Figure 2B.

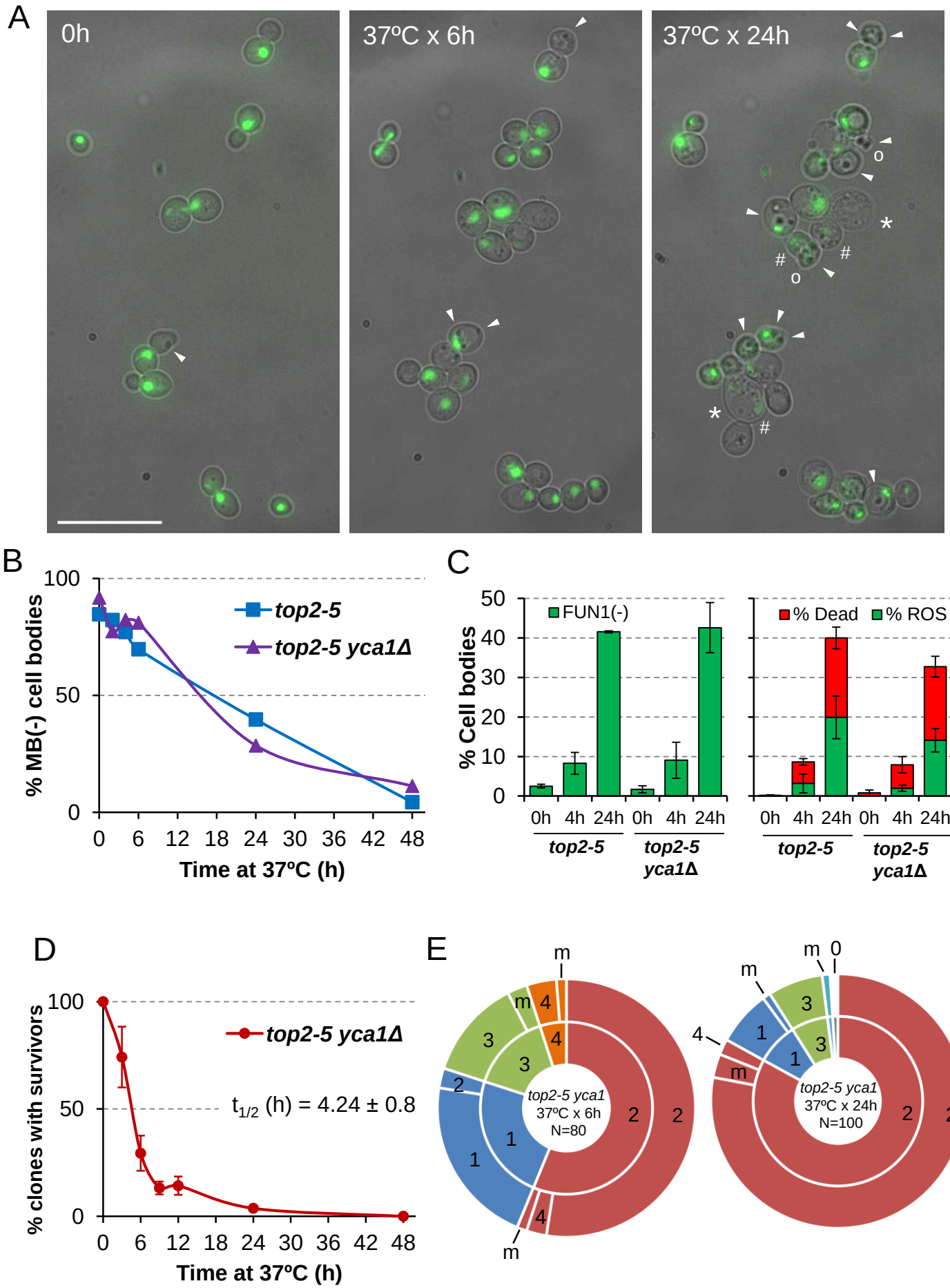
A
0h
37ºC x 6h
37ºC x 24h
B
% MB(-) cell bodies
top2-5
top2-5 yca1Δ
Time at 37ºC (h)
C
% Cell bodies
FUN1(-)
% Dead
% ROS
0h 4h 24h 0h 4h 24h
top2-5
top2-5 yca1Δ
D
% clones with survivors
top2-5 yca1Δ
t1/2 (h) = 4.24 ± 0.8
Time at 37ºC (h)
E
top2-5 yca1
37ºC x 6h
N=80
top2-5 yca1
37ºC x 24h
N=100

Figure 4. Cell vitality remain high for several hours after the *top2* mitotic catastrophe and is not modulated by Yca1. (**A**) Morphological patterns of cell and nuclear sickness after the *top2* MC. Haploid *top2-5 HTA2-GFP* cells were seeded onto agarose patches and the same fields visualized under the fluorescence microscope at 0 h, 6 h and 24 h after the 37 ºC temperature upshift. White filled triangles point to darkened inclusion bodies, asterisks (*) swelled cells, open circles (○) cells that has lost their rounded shape, and hash (#) points to cells that have largely lost the H2A-GFP signal. BF, bright field. Scale bar corresponds to 20 µm. (**B**) Time course of cell vitality decline as reporter by methylene blue (MB) negative staining. Asynchronous cultures of the *top2-5* and *top2-5 yca1*Δ strains were grown at 25 ºC before shifting the temperature to 37 ºC. At the indicated time points (0, 2, 4, 6, 24 & 48 h), samples were taken and stained with the vital dye MB. (**C**) Cell vitality decline as reported by metabolic competence, intrinsic ROS generation, and loss of plasma membrane impermeability. Cells were treated as in B and stained at the indicated time points with the vital dye FUN1, the death marker propidium iodide (PI), and/or the ROS reporter DCFH-DA (mean ± s.e.m., n=3). (**D**) Clonogenic survival profile of *top2-5 yca1*Δ as determined on the low-density plates (mean ± s.e.m., n=3). The experimental procedure is described in Figure 1C. (**E**) Ability to re-bud of the *top2-5 yca1*Δ MC progeny as determined on the high-density plates. The experimental procedure is described in Figure 2.

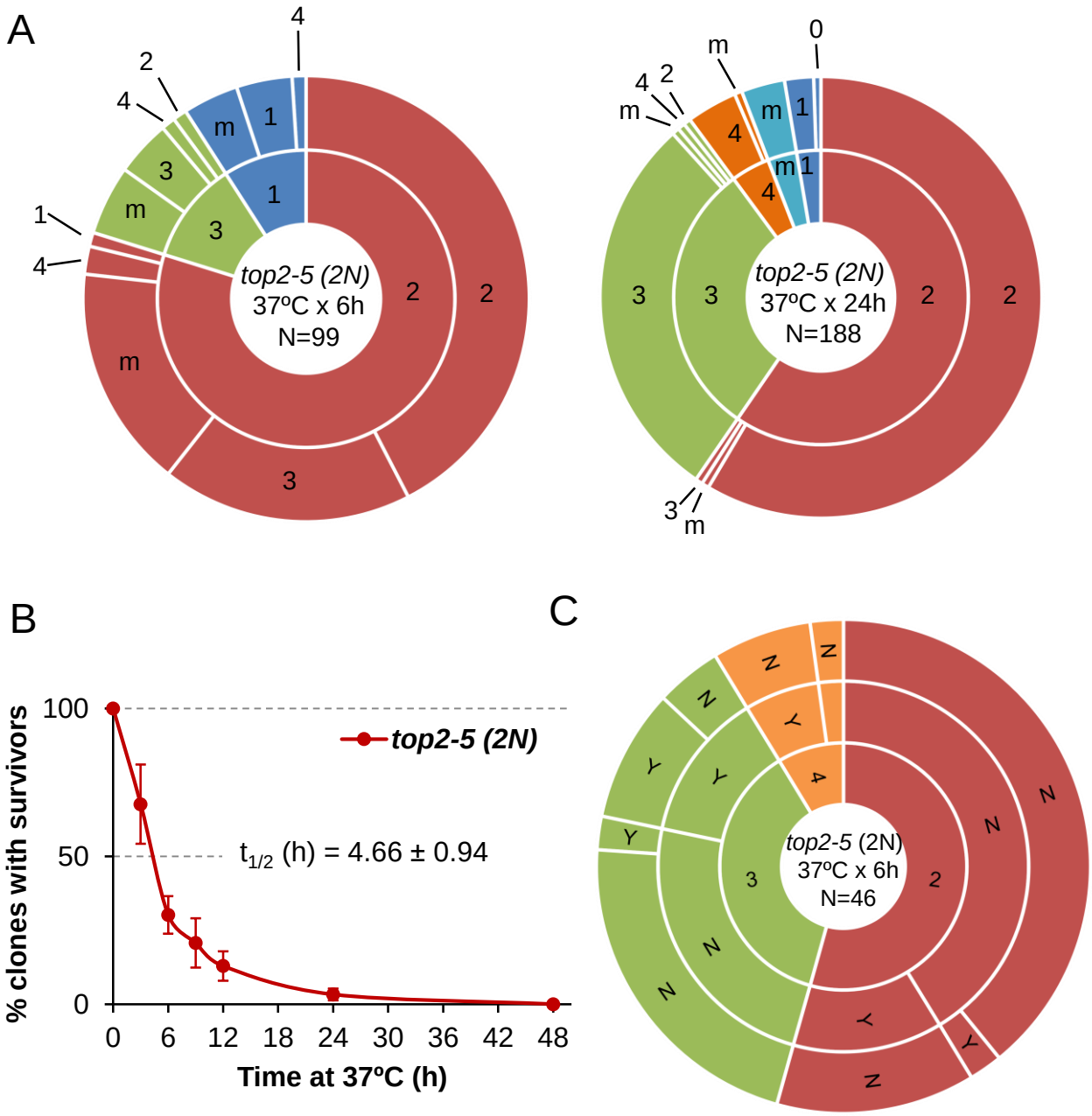

Figure 5. Mitotic catastrophe in *top2-5* diploids leads to progeny with a greater capacity for cell division than observed in the haploid. Isogenic homozygous *top2-5* diploid cells were grown and spread at either low or high cell density on Petri dishes. In addition, G_1/G_0 cells were micromanipulated, arrayed and treated as described in Figure 2C. (**A**) Ability to re-bud after transient (6 h or 24 h) incubations at 37 ºC of the high-density plates. The experimental procedure is described in Figure 2. (**B**) Clonogenic survival profile as determined on the low-density plates (mean ± s.e.m., n=3). The experimental procedure is described in Figure 1C. (**C**) Capability of the progeny to split apart and relationship with overall survivability. The experimental procedure is described in Figure 2C.

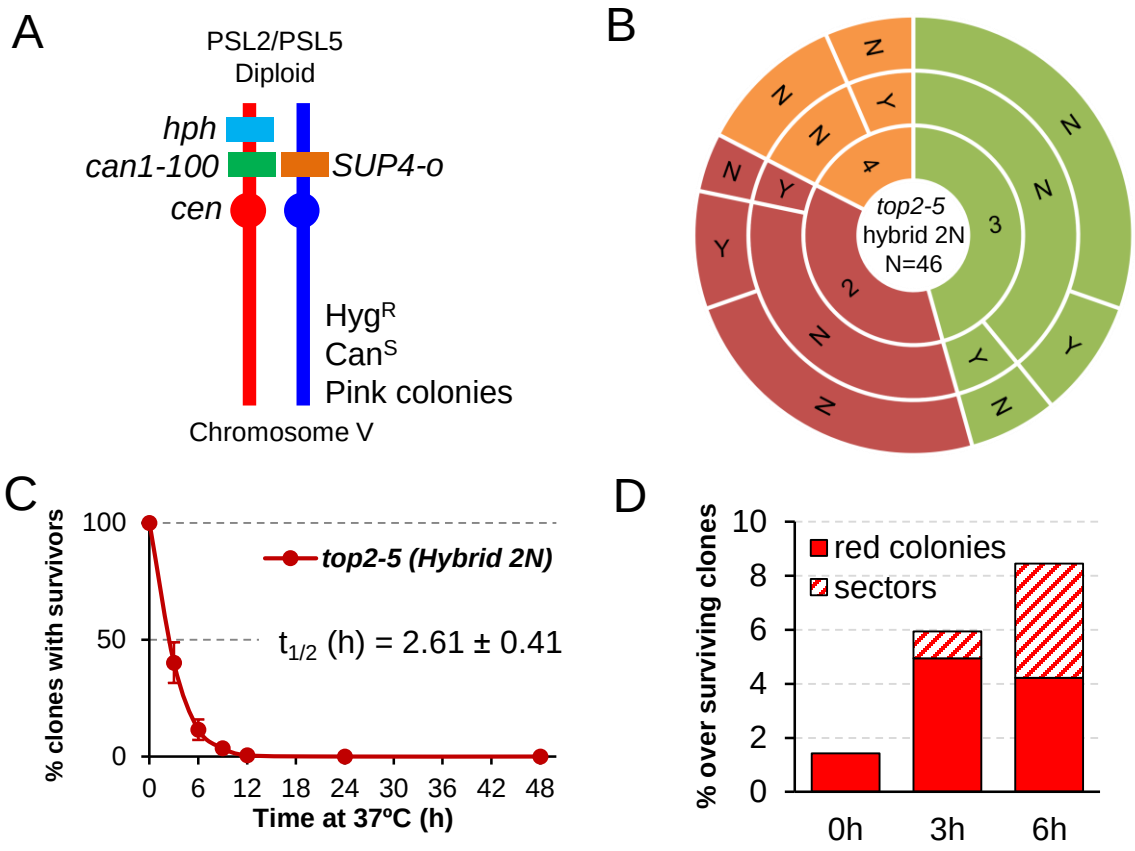

Figure 6. Mitotic catastrophe in *top2-5* heterozygous diploids leads to a genetically unstable progeny (I). (**A**) Schematic of the engineered chromosome V (cV) from the hybrid highly heterozygous (~55,000 SNPs) diploids used in this study. As explained in the text, the genetic modifications applied in cV allowed for selection of chromosome rearrangements. (**B**) G_1/G_0 cells from the hybrid highly heterozygous *top2-5* diploid FM1873 strain were micromanipulated, arrayed and treated as described in Figure 2C. The capability of the immediate progeny to split apart and its relationship with overall survivability is shown in the sunburst chart. The interpretation is described in Figure 2C. (**C**) Clonogenic survival profile of FM1873 as determined on low-density plates (mean ± s.e.m., n=3). The experimental procedure is described in Figure 1C. (**D**) Percentage of red or sectored (either white:red or pink:red) colonies in the surviving clones. Both outcomes often reflect genetic alterations on cV as described in the text.

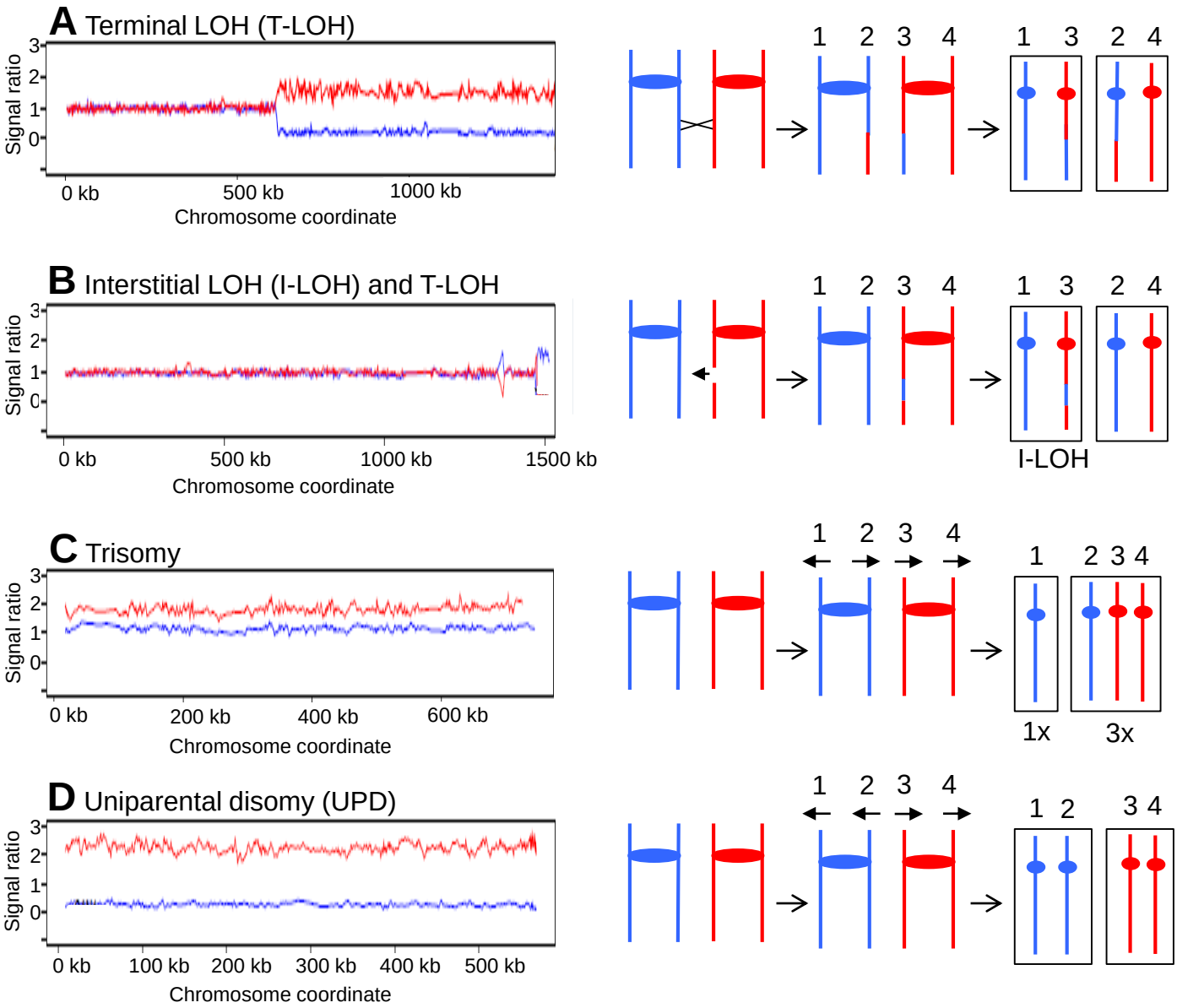

Figure 7. Genomic alterations detectable by microarrays. In this figure, the results of microarray analysis of colonies derived from FM1873 or MD684 are shown on the left side, and diagrams of the genetic events producing these patterns are shown on the right side. For the microarray patterns, hybridization to SNPs specific to homologs derived from W303-1A are shown in red, and hybridizations to SNPs specific to YJM789 are shown in blue. The X-axis shows SGD coordinates for the chromosome, and the Y-axis shows the ratio of hybridization normalized to a heterozygous diploid strain. (**A**) Terminal-LOH event on IV (MD684.1.1 (E1) in Table 1). Such events reflect either crossovers or BIR events. (**B**) Interstitial-LOH event (marked with arrow) plus T-LOH event on chromosome IV (FM1873-15c (C2) in Table 1). (**C**) Trisomy (MD684.1.1 (E1) in Table 1). This isolate has two copies of the W303-1A-derived chromosome XIV and one copy of the YJM789-derived XIV. (**D**) Uniparental disomy. This isolate has two copies of the W303-1A-derived chromosome V and no copies of the YJM789-derived chromosome.

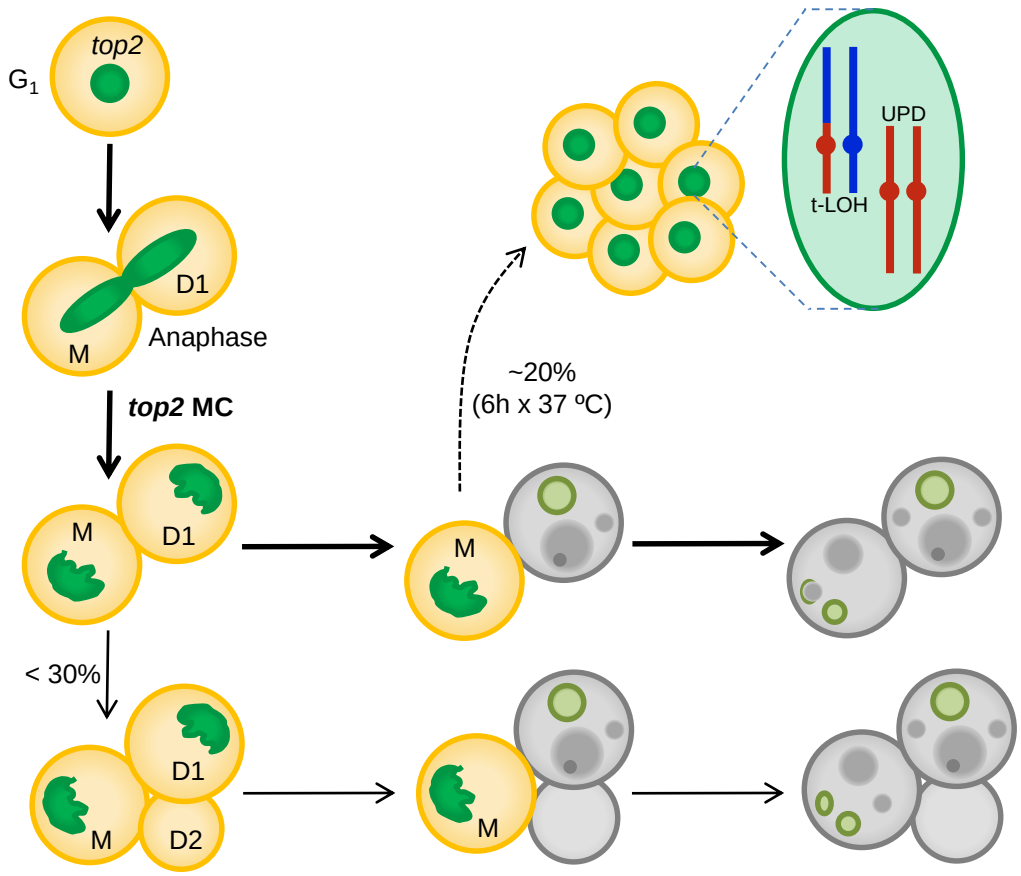

Figure 8. Summary of the *top2*-mediated mitotic catastrophe and the fate of the immediate progeny. After inactivation of Top2, cells cannot resolve sister chromatids in anaphase, leading to an anaphase bridges between the mother (M) and its daughter (D1). These bridges are quickly severed (at least in the *top2-5* mutant [36]). The immediate progeny coming from the *top2* mitotic catastrophes (MCs) is largely unable to enter a new cell cycle (do not re-bud) despite remaining metabolically active for many hours; hence, these cells become senescent. Only ~25% of the original mothers re-bud once (D2) after the *top2* MC. The long-term fate of these cells is death. Most, if not all, cells will eventually die through accidental cell death (ACD), as deduced from both the asynchrony and asymmetry of death events and the lack of regulation by the death modulator Yca1(Mca1). The inability to enter a new cell cycle is likely a consequence of both the massive DNA damage as a consequence of bridge severing, and the misdistribution of essential genetic material coded on the chromosome arms between the daughter cells. A small proportion of the progeny, especially those cell that underwent a milder *top2* MC (e.g., already in S/G_2 at the time of Top2 inactivation) survives to yield a population of cells with characteristic footprints of genomic instability. Two of these footprints, terminal loss of heterozygosity (T-LOH) and uniparental disomy (UPD) are expected outcomes from anaphase bridges.